Atmospheric Environment 378 (2026) 122061

Contents lists available at ScienceDirect

Atmospheric Environment

journal homepage: www.elsevier.com/locate/atmosenv

Seasonal and diurnal variability of fine aerosol sources derived from receptor modeling of multi-instrument online composition measurements in Athens, Greece

Georgios Grivas [a,*], Eleni Liakakou [a], Panayiotis Kalkavouras [a], Iasonas Stavroulas [a], Kalliopi Petrinoli [a,b], Despina Paraskevopoulou [a], Irini Tsiodra [a], Maria Tsagkaraki [b], Aikaterini Bougiatioti [a], Alessandro Bigi [c], Evangelos Gerasopoulos [a], Nikolaos Mihalopoulos [a,b,**]

[a] Institute for Environmental Research and Sustainable Development, National Observatory of Athens, Athens, 15236, Greece
[b] Environmental Chemical Processes Laboratory, Department of Chemistry, University of Crete, Heraklion, 71003, Greece
[c] Department of Engineering "Enzo Ferrari", University of Modena and Reggio Emilia, Modena, 41125, Italy

HIGHLIGHTS

- Diurnal cycles of $PM_{2.5}$ sources on a seasonal basis in Athens, combining online monitors.
- High-resolution data elucidate contrasts between exhaust and non-exhaust traffic sources.
- Urban background $PM_{2.5}$ from traffic decreased by 28% during the spring 2020 lockdown.
- The variability of toxic shipping emissions at a large port also traced at inland sites.
- Natural particles and aged aerosol form a $PM_{2.5}$ background difficult to regulate.

GRAPHICAL ABSTRACT

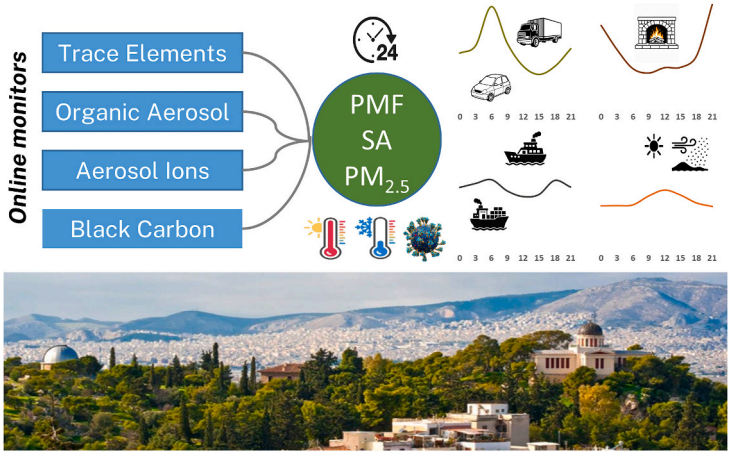

ARTICLE INFO

Keywords:
Particulate matter
Elemental composition
XRF
Source apportionment
PMF

ABSTRACT

To characterize the diurnal variability of fine aerosol sources on a seasonal basis, a monitoring campaign was conducted at the NOA-Thissio urban background site in central Athens. Online measurements were performed during warm (June-September 2019), cold (February-March 2020), and COVID-19 lockdown (March-May 2020) periods. Concentrations of 15 elements in $PM_{2.5}$ were measured at 3-h resolution with a Horiba PX-375 EDXRF analyzer. Collocated data were obtained for organic aerosol and ions (Q-ACSM), black carbon and its components

* Corresponding author.
** Corresponding author. Institute for Environmental Research and Sustainable Development, National Observatory of Athens, Athens, 15236, Greece.
E-mail addresses: ggrivas@noa.gr (G. Grivas), nmihalo@noa.gr (N. Mihalopoulos).

https://doi.org/10.1016/j.atmosenv.2026.122061
Received 2 January 2026; Received in revised form 19 March 2026; Accepted 2 May 2026
Available online 4 May 2026

Risk assessment
Lockdown

(AE33 aethalometer), and selected cations (PILS-IC). Metals related to non-exhaust emissions (Cu, Fe, Zn) exhibited bimodal cycles and substantial lockdown reductions (39-44%). Levels of crustal elements (Si, Al, Ti, Mn) were elevated at midday in summer due to enhanced dust erosion and resuspension. Episodic elemental concentrations were observed during Saharan dust outbreaks, wildfires (through emission and pyroconvection), and firework events. The speciated data were combined in PMF receptor modeling, identifying eight $PM_{2.5}$ factors related to traffic emissions (exhaust and non-exhaust), biomass burning (BB), oil combustion in shipping, natural particles (long-range transported and local), and secondary aerosol (regional and locally processed). Substantial lockdown decreases in traffic sources were observed (−28% combined), but only the evening peak in diurnal cycles was fully suppressed by the traffic ban. For the shipping source, the diel variation of passenger ship emissions appeared to build upon a strong background from commercial shipping. The results corroborate ongoing research in Athens, which indicates that achieving the new $PM_{2.5}$ standard will require further control of traffic emissions, proactive regulation of residential BB, and reevaluation of the urban impacts of heavy-oil combustion in shipping, considering the declaration of the Mediterranean as an emissions control zone.

1. Introduction

Fine aerosols originate from anthropogenic and natural emissions, either as primary particles or through the secondary processing of gaseous precursors. Organic aerosol (OA), black carbon, major inorganic ions, and dust make up most of the particulate matter (PM) mass. However, there are hundreds of highly toxic aerosol components, including several trace metals (Hu et al., 2012). Among regulated pollutants, $PM_{2.5}$ causes the most severe health effects from both short- and long-term inhalation exposure (e.g., 240,000 premature deaths in EU27 in 2022) (European Environment Agency, 2024). There is consistent epidemiological evidence on causal relationships linking $PM_{2.5}$ exposure with total and cardiovascular mortality (Di et al., 2017; Liu et al., 2019a), and outcomes like myocardial infarction, heart failure, and stroke (Desouza et al., 2021; Fisher et al., 2019; Krall et al., 2018). In this context, the EU has recently established for the first time a daily $PM_{2.5}$ limit value (25 μg m^{-3}) and lowered the annual standard by 60% (to 10 μg m^{-3}) in its updated air quality directive (EU 2024/2881).

Due to the heterogeneous composition of aerosols, it is challenging to identify the factors that drive their toxicity. Plausible pathways to short-term outcomes are centered on systemic inflammation and oxidative stress, which can be mediated by redox-active trace metals (Fang et al., 2015; Orach et al., 2021). Still, results from $PM_{2.5}$ composition- and source-based epidemiological studies remain inconclusive (Chen et al., 2020; Ostro et al., 2016). Little is known about the importance of sub-daily exposure, with some controlled human exposure experiments reporting cardiorespiratory effects after a few hours of exposure to ambient $PM_{2.5}$ (Hemmingsen et al., 2015; Vieira et al., 2016; Wyatt et al., 2020). Therefore, high-resolution aerosol composition data in urban areas are essential for assessing the value of regulating PM on a sub-daily basis.

In addition to aerosol composition data, quantitative information on contributions of local and regional sources is crucial in the evolving EU emissions landscape. Stationary fossil fuel combustion is decreasing under clean energy transition policies, while tailpipe emissions will be gradually curtailed and eventually superseded by non-exhaust emissions (Harrison et al., 2021). Indeed, the recent global lockdowns during the COVID-19 pandemic revealed substantial benefits of limiting urban road transport (Venter et al., 2020). Meanwhile, episodic sources are gaining importance (Pandis et al., 2016). The past decade's recession has increased the reliance of households on affordable biomass burning (BB) for heating, a largely unregulated source in the EU that contributes to severe pollution events. Furthermore, the increasing frequency and intensity of peri-urban wildfires are emerging as a major issue for summer air quality in climate-sensitive regions, such as the Mediterranean (Aguilera et al., 2021; Kaskaoutis et al., 2024). Therefore, source apportionment at high temporal resolution is essential for developing focused action plans rather than relying on broad measures.

The Southern European metropolis of Athens presents a case where characterizing fine aerosol sources at high temporal resolution is crucial. The large vehicle fleet is among the oldest in the EU, and shipping emissions affect even inland locations (Fragkou et al., 2025; Möring-Martínez et al., 2025), while natural and road dust can contribute substantially to the fine PM fraction. In recent years, residential BB has been the focus of aerosol research in Athens due to the intensity of nighttime smog events (Tsiodra et al., 2024). In addition to local sources, regional transport accounts for a large fraction of $PM_{2.5}$ (Gerasopoulos et al., 2011). Several filter-based $PM_{2.5}$-PMF studies have been conducted in the Greater Athens Area (GAA) (e.g., Amato et al., 2016; Grivas et al., 2018), but at best with 12-h resolution (Theodosi et al., 2018).

While filter-based PM source apportionment is typically resource-limited to daily samples, several online methods enable PM speciation and receptor modeling on shorter timescales. These include online X-Ray Fluorescence (XRF) spectrometers (Sofowote et al., 2014), single-particle spectrometers (Bi et al., 2011), online ion chromatographs (IC) (Makkonen et al., 2012), aethalometers (Briggs and Long, 2016), and various mass spectrometers for OA composition (Ng et al., 2010; Sun et al., 2025). As no single method can provide the full range of components required to source-apportion PM mass online (Cheung et al., 2024), it has long been recognized that a combination of methods is necessary (Buset et al., 2006; Li et al., 2004).

Trace element data are fundamental for PM source apportionment, since certain metals serve as markers for sources that would otherwise be difficult to characterize (e.g., non-exhaust vehicular emissions, heavy oil combustion, industrial emissions) (Yu et al., 2019). They can also support source-specific oxidative potential (OP) apportionment and health risk assessment (Camman et al., 2024; Campbell et al., 2024). High-resolution measurements of elemental composition are today possible using novel multi-metal analyzers, such as the Horiba PX-375 (Asano et al., 2017; Creamean et al., 2016) and the Sailbri Cooper Xact 620/625/625i (Bhowmik et al., 2022; Furger et al., 2017; Sofowote et al., 2014; Tremper et al., 2018) energy dispersive XRF (EDXRF) monitors. Several studies have assessed trace element levels and diurnal variations, or performed source apportionment, using online elemental speciation datasets (the majority of which were obtained with Xact analyzers) (Chang et al., 2018; Hasheminassab et al., 2020; Manousakas et al., 2022). Limited results are available from PX-375 measurements, all based on short-term campaigns (Ito and Miyakawa, 2023; Lopez et al., 2023; Mach et al., 2021, 2022; Miyakawa et al., 2023; Trebs et al., 2024), and only one study performed source apportionment with the metals dataset (Ahmad et al., 2025). Some studies have integrated data from online XRF analyzers with other aerosol monitors (e.g., ACSM, aethalometer, online OC/EC, ionic composition analyzers) in a common receptor modeling framework to characterize an expanded range of fine aerosol sources (Belis et al., 2019; Liu et al., 2019b; Su et al., 2020; Windell et al., 2024). Most of these works rely on short-term campaigns, whereas time-extended datasets (lasting more than three months) that reflect seasonal variability are scarce (Jeong et al., 2022). Recently, results from an integrated Xact-ACSM-Aethalometer source apportionment study were reported for a suburban background location in the GAA, based on measurements of monthly duration and emphasizing the

methodological aspects of the real-time modelling framework (Manousakas et al., 2025).

The present study focuses on high-resolution chemical composition characterization and source apportionment of fine aerosol on an extended seasonal basis, combining data from four online aerosol monitors (PX-375 EDXRF metals analyzer, ACSM, 7-λ aethalometer, PILS ion analyzer) operated at the NOA-Thissio site in central Athens. Measurements were conducted over six months in 2019-2020, including the spring 2020 COVID-19 lockdown period. Fine aerosol composition data at high temporal resolution (3-h intervals) were integrated into PMF receptor modeling. The temporal variability of the chemical composition and source contributions was assessed at short (diurnal, weekly) and longer (seasonal) scales, probing also the effects of specific events (wildfire, dust transport, fireworks, BB smog episodes, lockdown). In this process, important insights into the contributions and diurnal variability of local/regional sources, as well as their toxicity, were gained, which can provide a baseline for future research and can inform air quality management and exposure-prevention strategies in the GAA.

2. Methodology

2.1. Study area, monitoring site and periods

2.1.1. Study area

The Greater Athens Area (GAA) in the Attica region (Fig. S1), with 3.6 million residents (2021 census), is the largest urban agglomeration in Southeastern Europe, as well as the ninth-largest and third-most densely populated in the EU. The central Athens basin hosts most of the GAA population (3.1 million), and the car parc in the Attica region comprises approximately 4.0 million vehicles, of which the majority (2.5 million) are gasoline-powered private cars. The share of diesel passenger cars increased after the 2011 removal of a long-standing ban in Athens. Still, it remains relatively low (≈10%) compared to other EU cities (Fameli and Assimakopoulos, 2015), and most of these vehicles are new-technology Euro 5 and Euro 6 models. The majority of road diesel mileage in the GAA is attributed to commercial light- and heavy-duty diesel vehicles (about 0.3 million). While Greece has the 4th-oldest passenger-car fleet in the EU, its heavy-duty vehicle (HDV) and bus fleets are the oldest (Spyropoulos et al., 2022).

Following the Greek sovereign debt crisis of the previous decade, which led to income loss and still-standing excise taxes on heating oil, the use of biomass for domestic heating increased sharply (Theodosi et al., 2018). Meanwhile, heating oil consumption in Attica dropped by nearly 60% between 2011 and 2018 (Tsiodra et al., 2021). A recent survey estimated that biomass burning in fireplaces and stoves has become the primary heating source for more than 10% of homes in Attica (Fameli et al., 2021). This previously negligible share (Grivas et al., 2012) is now apparently sufficient to drive extreme winter nighttime smog events (Tsiodra et al., 2024). The heating season in Attica runs from November through April, with the demand peaking between December and March (Fameli et al., 2021). The GAA is a major commercial and transportation hub in Southern Europe, encompassing the Piraeus port zone, which manages the highest passenger traffic in Europe and the largest container throughput in the Mediterranean (Li et al., 2021). Passenger vessel traffic in the Piraeus port area intensifies during the warm season, corresponding to the peak tourist season (Stavroulas et al., 2021; Tritsarolis et al., 2022).

The topography of the Athens basin, surrounded by medium-altitude ranges and opening to the sea in the S-SW, promotes mesoscale circulation and frequent stagnation episodes. Sea-breeze advections from the south, which are strong and effective from morning until late afternoon in the warm months, can also be observed during October-April in the central-southern parts of the basin around midday. Strong synoptic-scale winds are common year-round, with the difference that during the cold season they have limited daily variability, whereas the summer regime ("Etesians") is mainly diurnal and can even affect the central-southern part of the basin (Kalkavouras et al., 2020; Kassomenos et al., 1998). The mixing layer height (MLH) climatology, assessed from ceilometer observations (Petrinoli et al., 2025), indicates that the monthly mean MLH in June-September ranges from 900 to 1000 m, whereas in the cold period it is much shallower (e.g., 600-800 m in February-March).

2.1.2. The NOA-Thissio Air Monitoring Station

Measurements of aerosol chemical composition were conducted at the NOA-Thissio site (THI) in central Athens (37.9732° N, 23.7180° E, 105 m a.s.l.; Fig. S1). This is an urban background site, located in a residential area (≈11,000 km^{-2} population density) in the central part of the Athens basin, about 500 m from the nearest primary road, yet still affected by road transport emissions (Liakakou et al., 2020; Theodosi et al., 2018). Traffic volume in Athens declines in the summer (Fig. S2), particularly during the August vacation period (Kalkavouras et al., 2024). HDV circulation is neither prohibited nor uncommon in central Athens, particularly in the commercial areas N-NW of the site (Chasapi et al., 2025). During the heating period, the site is heavily impacted by residential BB in central Athens (Tsiodra et al., 2024, and references therein). Moreover, NOA-Thissio is a receptor for oil-combustion emissions from shipping activity in and around the Piraeus port, located 7 km southwest (Theodosi et al., 2018; Tsiodra et al., 2021).

2.1.3. Study periods

The study focused on three periods: warm (June 19, 2019 – September 14, 2019), cold (February 26, 2020 – March 22, 2020), and lockdown (March 23, 2020 – May 10, 2020). Measurements continued through May 18, 2020, but the post-lockdown period was brief and dominated by a major Saharan dust transport episode (Kokkalis et al., 2021). Strong Saharan dust intrusions were also observed in March. The cold period, although in late winter, had a mean temperature of 13.6 °C, indicating strong heating demand (Fameli et al., 2021). Typical meteorological conditions (Table S1) prevailed during the warm period; however, it was punctuated by two wildfire events on July 4-6 and August 13-14, which transported plumes from Euboea in the NE. The latter burned more than 2500 ha of pine forest in 40 h (Giannaros et al., 2020), and its convective plume significantly affected air quality in the Athens basin (Stavroulas et al., 2020). The lockdown period (Grivas et al., 2020) began with the imposition of a national lockdown that prohibited the use of private vehicles except for commuting to work and health facilities. Public transportation schedules became sparser and confined to daytime, while all outdoor civilian activity was restricted between 21:00 and 6:00 ("curfew"). Under these rare circumstances, the entire GAA population stayed at home also during the Easter weekend (April 18-19, 2020) (Stavroulas et al., 2024). Wind intensity, humidity, and precipitation were similar during the cold and lockdown periods, enabling a meaningful assessment of the lockdown effects for most aerosol parameters and sources. The statistical assessment of cold-lockdown differences (Table S1) indicates that for the parameters most important for aerosol dynamics (wind speed and precipitation), the differences between the cold and lockdown periods were not statistically significant at the 0.05 level (p: 0.86 and 0.83, respectively). For relative humidity and solar radiation, the differences were again not statistically significant (p: 0.11 and 0.06, respectively). As expected, temperatures were significantly higher during the spring lockdown, but this period was relatively colder in 2020 than in the previous 4 years (15.9 vs. 17.6 °C) (Grivas et al., 2020). All times appearing in the manuscript refer to local time (LT).

2.2. Instrumentation for online aerosol composition monitoring

$PM_{2.5}$ elemental composition (15 elements: Al, As, Ca, Cr, Cu, Fe, K, Mn, Ni, Pb, S, Si, Ti, V, and Zn) was determined using an online EDXRF monitor (PX-375, Horiba Inc., Kyoto, Japan) (Asano et al., 2017; Creamean et al., 2016). The same instrument also provided $PM_{2.5}$

concentrations using its built-in beta-attenuation monitor (sampling at 16.7 l min^{-1}, reel-to-reel on a PTFE filter tape with two-layer nonwoven backing, through a heated inlet line). The PX-375 monitor was operated in 3-h sampling cycles to ensure sufficient quantification of metals above detection limits (Miyakawa et al., 2023; Zhang et al., 2024), yielding 1290 samples over the entire monitoring period. X-ray intensity was calibrated using NIST Standard Reference Material (SRM) 2783. Detection limits (DL) were determined as three times the standard deviation of ten measurements obtained after placing a zero filter in the inlet line (Table S2). With the exception of As and V, all other elements were detected above the DL in more than 50% of the samples.

The major non-refractory (NR) components (OA, SO_4^{2-}, NO_3^-, NH_4^+, Cl^-) in submicrometer aerosol were measured every 30 min by a Quadrupole ACSM (Aerodyne Inc., Billerica, MA, USA), following flash volatilization and electron impact ionization (Freney et al., 2019; Ng et al., 2011). The concentrations of the *m/z* 60 fragment, which represents decomposition products of compounds emitted during biomass pyrolysis, such as levoglucosan, were also used. Details on ACSM measurement, calibration, and QA/QC at the site are provided by Stavroulas et al. (2019). Positive Matrix Factorization (PMF) (Crippa et al., 2014) was performed on the OA mass spectra using the SoFi Pro toolkit (Canonaco et al., 2013, 2021). OA was decomposed into five components. Primary OA sources (Hydrocarbon-like OA – HOA, Biomass Burning OA – BBOA, and Cooking OA – COA) were constrained using reference anchor profiles (Crippa et al., 2013; Ng et al., 2010), verified by multiple studies at the same site (Stavroulas et al., 2019, 2024). Two unconstrained secondary OA (SOA) factors (Less-Oxidized Oxygenated OA – LO-OOA, More-Oxidized Oxygenated OA – MO-OOA) were also resolved. More details are provided in Section S1 of the supplement. The OA components were used as external variables to validate the PMF solution.

Equivalent black carbon (hereafter BC) concentrations in $PM_{2.5}$ were determined by filter-based aerosol absorption measurements at seven wavelengths (370 – 950 nm), every 1 min, using an AE33 aethalometer (Magee Scientific, Berkeley, CA, USA) with DualSpot compensation for filter loading effects (Drinovec et al., 2015; Liakakou et al., 2020; Savadkoohi et al., 2023). Brown Carbon (BrC) absorption at 370 nm was estimated using the BrC model that assumes a unity Absorption Ångström Exponent (AAE) for "pure" chemical BC and zero BrC absorption at 880 nm (Kirchstetter and Thatcher, 2012). Contributions from source-specific BC components related to fossil-fuel combustion (BC_{ff}) and biomass burning (BC_{bb}) were also estimated using the Aethalometer model (Sandradewi et al., 2008), with site-specific, optimized AAE for BC_{ff} and BC_{bb} absorption (1.11 and 1.72, respectively) (Savadkoohi et al., 2025). A particle-into-liquid-sampler coupled with an Ion-Chromatography system (PILS-IC) was used to determine the concentrations of major fine aerosol cations (three measurements per hour) (Fourtziou et al., 2017; Weber et al., 2001). Data on Na^+ and Mg^{2+} concentrations were included in the analysis, aiming to represent sea-salt particles in the receptor model, which was not possible with the other instruments. All aerosol composition data – and subsequently presented ancillary data – were averaged to the 3-h measurement intervals of the PX-375 analyzer (starting at midnight, local time).

2.3. Ancillary data and QA/QC

24-hr $PM_{2.5}$ samples were collected on Quartz filters daily throughout the measurement period, using reference-equivalent low-volume samplers. All samples were analyzed for organic and elemental carbon (OC, EC) with a thermal-optical transmission Sunset analyzer (Sunset Laboratory Inc., Portland, OR, USA), and for water-soluble ions (including SO_4^{2-}, NO_3^-, NH_4^+) by ion chromatography (IC; Dionex DX-500; Thermo Fischer Scientific, Waltham, MA, USA). Moreover, a subset of warm-period samples (June 19 to July 8) was analyzed for major and trace elements using inductively coupled plasma mass spectrometry (ICP-MS; NexION 300X, PerkinElmer Inc., Waltham, MA, USA) (Theodosi et al., 2018). Comparisons between daily-averaged elemental concentrations quantified by ICP-MS and those measured by online ED-XRF are summarized in Table S2, in terms of Deming no-intercept regression slopes (henceforth slopes) and squared correlation coefficients. With the exception of V and As, the results indicate good linearity and acceptable biases for the other metals, with r^2 values of 0.73-0.99 and slopes of 0.66-1.33. The sulfur concentrations by the PX-375 were strongly correlated with filter-based sulfate ($r^2 = 0.91$) and ACSM-sulfate ($r^2 = 0.78$). A recent study that systematically compared PX-375 and ICP-MS daily measurements is consistent with the present findings, reporting, inter alia, a high rate of BDL values for As and a large underestimation of V by the online monitor (Windell et al., 2025). Due to the substantial uncertainty in the determination of V and As, and the large share (>75%) of BDL data, they were excluded from subsequent analyses (Furger et al., 2017).

Moreover, intercomparisons of nitrate and ammonium concentrations measured by ACSM and IC in $PM_{2.5}$ filters showed strong correlations (r^2: 0.80 for NO_3^- and 0.77 for NH_4^+) and ACSM/IC slopes close to unity (0.91 for NO_3^- and 0.90 for NH_4^+). Therefore, the methodological bias arising from their inclusion as submicron, non-refractory components in PMF source apportionment of $PM_{2.5}$ should be limited, as their participation in the intermodal range (1-2.5 μm) is known to be small in Athens (Theodosi et al., 2011). Finally, the EC-over-BC regression produced a slope of 0.90 and an r^2 of 0.85. BC concentrations were also measured during the 2020 period using a Multi-Angle Absorption Photometer (MAAP; model 5012, Thermo Fisher Scientific Inc.), which actively compensates for aerosol scattering ($r^2 = 0.99$; MAAP/AE33 slope = 1.08). To further assess the biases introduced by merging NR-PM_1 ACSM data in $PM_{2.5}$ source apportionment, mass closure analysis was performed (details in Section S2) based on the calculation of carbonaceous aerosol, secondary inorganic aerosol, dust, and sea salt components from the speciation datasets (Chow et al., 2024). The results indicate a satisfactory reconstruction (least-squares regression r^2: 0.86; measured-over-reconstructed slope: 0.85; intercept: 2.8 μg m^{-3}) (Fig. S3). The non-reconstructed fraction (probably linked to intermodal ammonium and nitrate salts, and primary biogenic organics) was small (4.3%, 0.6 μg m^{-3}). Similar results have been reported in past $PM_{2.5}$ mass closure analyses at THI (Theodosi et al., 2018).

Concentrations of gaseous species were also measured continuously at the site, including CO and CO_2 (cavity ring down spectroscopy; G2401, Picarro Inc., Santa Clara, CA, USA), nitrogen oxides (chemiluminescence; Serinus 40, Ecotech, Melbourne AU) and O_3 (UV–Vis; mod. 49i, Thermo Fisher Scientific, Waltham, MA, USA) (Grivas et al., 2020). Additional data (SO_2 and coarse particle concentrations: PM_c) were retrieved from regulatory stations in central Athens (Fig. S1). Meteorological data were also available on site (Table S1). 5-day back-trajectories were calculated using the Hybrid Single-Particle Lagrangian Integrated Trajectory model (HYSPLIT-4, NOAA) (Stein et al., 2015) for air masses arriving every 3 h at 500 m above ground, corresponding to mixing within the boundary layer (Dimitriou et al., 2021).

2.4. Source apportionment using the online aerosol composition dataset

Combined $PM_{2.5}$ source apportionment – using metals, ions and carbonaceous components from different online instruments – was conducted using the PMF5.0 model, based on the ME-2 program (Belis et al., 2019; Hong et al., 2021; Li et al., 2024; Liu et al., 2022; Liu et al., 2019b; Windell et al., 2024; Zhang et al., 2019a,b). The species considered in the PMF analysis included 13 out of the 15 PX-375 elements (omitting As, V), ammonium, sulfate, nitrate, non-refractory chloride, and *m/z* 60 from the ACSM, BC from the aethalometer, as well as Na^+ and Mg^{2+} from the PILS-IC system. A PMF application combining data from an online metals analyzer, an ACSM (OA, ions, selected *m/z* fragments) and an aethalometer is also detailed in Su et al. (2020). $PM_{2.5}$ measured by the PX-375 was set as the total variable.

Firework events were excluded from the PMF dataset, since such occurrences on a large scale are very infrequent in the GAA, and the small number of impacted samples precluded taking alternative PMF approaches to apportion the source (Camman et al., 2024; Rai et al., 2020).

Uncertainties for trace elements were calculated based on detection limits (DL) and precision (Reff et al., 2007). To estimate the fractional precision of measurements, three separate components were considered (Windell et al., 2025). First, the repeatability of the measurement method should be assessed. To date, no studies have reported results from the concurrent operation of PX-375 monitors. Therefore, the reference relative precision (u_R) data reported by Trebs et al. (2024) were used. These values were calculated from repeated measurements of multi-element reference materials with mass loadings representative of polluted conditions. Second, the uncertainty of the reference material (u_{RM}) used to calibrate PX-375 (NIST 2783) was included as a fractional error term (NIST, 2011). Flow rate uncertainty (u_{FL}: 1.2%), as stated by the manufacturer, was also accounted for. Overall, the uncertainty of a PX-375 concentration measurement i for element j (x_{ij}) was calculated as:

$$u_{ij} = \sqrt{\left(DL_j/2\right)^2 + \left[\left(u_{Rj} + u_{RMj} + u_{FL}\right) \times x_{ij}\right]^2}$$

The mean fractional attribution of the four uncertainty components to the total mean value is shown in Fig. S4 for each element included in the PMF analysis. It appears that for the majority of metals measured by the PX-375 monitor, with the exception of major elements S, Fe and Ca, the largest portion of the uncertainty (>50%) was attributable to the detection limit.

Uncertainties for the major ACSM components considered in the PMF analysis were estimated using the same approach, based on detection limits (DL) and fractional precisions (Dai et al., 2021; Kalkavouras et al., 2024). The reference detection limits reported by Ng et al. (2011) and the reproducibility estimates from the Europe-wide Q-ACSM intercomparison experiments by Crenn et al. (2015) were applied (Belis et al., 2019). For m/z 60, the instrument-reported uncertainties were used. The uncertainty of BC was set to 15% for 30-min average data, according to Via et al. (2023). Finally, the uncertainties for the two PILS cations were based on method detection limits calculated from blank measurements, and precisions as reported by Orsini et al. (2003). Standard propagation methods were followed to calculate uncertainties at 3-h intervals. The PMF solution selection and validation strategy is summarized in Section S3 of the supplement. Details on the PMF database, and on the selection, performance, constraining, and error evaluation of the selected PMF solution (Brown et al., 2015) are provided in Table S3 and Fig. S5.

2.5. Evaluation of potential risks from diurnal exposure to concentrations of trace metals

The source apportionment results for potentially toxic elements (Cr, Ni, Pb, Mn, Cu, Zn, Al) were used to gain insights into the relative carcinogenic and non-carcinogenic source impacts and the associated sub-daily exposure risk patterns (Hamad et al., 2016; Janta et al., 2025). Such a risk assessment approach at the diurnal level, supported by the availability of high-resolution elemental data, has only recently been applied (Chen et al., 2021; Lakra et al., 2026). Here, lifetime hazard indices (HI) and cancer risks (CR) were not explicitly estimated, as the focus was on sub-daily variability rather than on lifetime risk assessment (which would require longer-term data with full annual coverage, while also considering that personal exposure varies by time of day and activity patterns).

Instead, the variables $\sum_i C_i/RfC_i$ and $\sum_i C_i{*}IUR_i$ were calculated, where C_i is the source-specific concentration of metal i (at 3-hr mean resolution), RfC_i is the Reference Concentration for non-carcinogenic exposure to the metal, and IUR_i is the respective carcinogenic Inhalation Unit Risk. The relative source attribution of the two parameters is the same as if HI and CR were estimated, as all further calculations are proportional (according to the selected exposure parameters) (Hu et al., 2012). The above values, initially calculated for each PMF factor, were then multiplied by the normalized factor contributions to obtain source-specific diurnal cycles for the warm and cold periods separately. Finally, the two period-specific cycles were averaged to provide a more reliable estimate of long-term exposure.

A detailed presentation regarding the selection of toxicological parameters (RfC, IUR, adjustments for oxidation state, and compound-specific potency) is provided in Section S4 and Table S4. RfC values were available for 7 of the elements (Cr, Ni, Pb, Mn, Cu, Zn, Al) used in the PMF analysis, while 3 elements (Cr, Ni, Pb) were considered in the assessment of carcinogenic risks. These values were primarily obtained from the EPA IRIS system (EPA, 2025) and additional resources, including the EPA PPRTV (Provisional Peer-Reviewed Toxicity Values) database, the EPA RSEI (Risk-Screening Environmental Indicators) database, and the California Office of Environmental Health Hazard Assessment (OEHHA).

3. Results and discussion

3.1. Levels and temporal variability of elemental concentrations

Even with the inclusion of the lockdown period and the absence of measurements during peak BB conditions (December-January), the overall average $PM_{2.5}$ concentration was considerably higher than 10 μg m^{-3} (15.8 ± 6.0 μg m^{-3}), with 12 daily exceedances of 25 μg m^{-3} (7.5% frequency, higher than mentioned in the EU 2024/2881 directive). Based on the average of cold- and warm-period mean concentrations (to partially compensate for unequal sample sizes), the mean Ni concentration (1.0 μg m^{-3}) was well below the long-term target value of 20 μg m^{-3} specified in the directive. Ni has been acknowledged as a shipping-emission tracer at sites within the Athens basin (Grivas et al., 2018; Theodosi et al., 2018). Despite the increase in cargo shipping activity at the Piraeus port over the previous decade (Kalkschmied and Stricker, 2026), fine-particle Ni concentrations appear to have decreased relative to the annual mean urban background concentration (2-2.5 μg m^{-3}) in 2010-2012, determined by filter-based EDXRF analyses (Grivas et al., 2018; Tsai et al., 2015). The mean Ni concentration was also lower (by almost 30%) than values reported for 2013-2014 (1.5 μg m^{-3}) at a suburban site deeper in the Athens basin (Amato et al., 2016; Manousakas et al., 2021). The results likely indicate the benefits of regulating at-berth and coastal shipping emissions over the last decade (Saliba et al., 2021; Sorte et al., 2020). The absence of the high-winter period is not expected to affect these variation patterns as shipping activity in the Greek maritime waters is reduced during these months (Poupkou et al., 2026). Concentrations of traffic-related Cu and Zn also appear to have declined (by 50-60%) in the urban background of Athens since 2011 (Grivas et al., 2018), but in 2019-2020 were still comparable to those reported for the suburban background six years prior (Amato et al., 2016). Even with potential underestimations by the PX-375 monitor (Table S2) and the absence of the higher-traffic winter period, this decrease is substantial and is likely related to regulations for fossil fuel combustion and industrial emissions at a regional level (Upadhyay et al., 2025; Veld et al., 2021), as traffic volumes in Athens did not change (Spyropoulos et al., 2022). This is supported by the apparent decline in S levels (from 1.6 to 1.0 μg m^{-3}), compared to a GAA-wide study that used EDXRF measurements in 2010-2011 (Tsai et al., 2015).

Fig. S6 displays the percentage change of period-mean concentrations relative to the full-period average (excluding major dust events, wildfires, and fireworks, which are discussed in Section 3.2). The concentrations of crustal elements (Al, Si, Ti) showed a warm vs. cold period enhancement due to more intense aeolian erosion, resuspension from drier surfaces, and the absence of precipitation (Clemente et al., 2023). Conversely, Fe was not affected, in view of the additional contribution from road-transport, while large cold- vs. warm-period increases were

observed for non-exhaust tracers (Cu: 38%, Zn: 21%), due to the intensification of traffic in a shallower boundary layer. The highest cold-period enhancement (more than two-fold) was observed for K emitted by extensive residential BB (Theodosi et al., 2018). Ni showed higher levels during the warm period (Pey et al., 2013), consistent with increased passenger shipping in Piraeus. The International Maritime Organization (IMO) 2020 global sulfur cap entered into force in January 2020 and may have led to immediate reductions in shipping emissions (Song et al., 2022); however, assessing its impact on the observed seasonal pattern is difficult. The lockdown resulted in decreases (compared to the preceding cold period) for all anthropogenic elements (Fig. S6), primarily for those affected by traffic restrictions (Cu, Zn, Fe, Pb; by 31-44%) (Clemente et al., 2022; Hicks et al., 2021; Jeong et al., 2022). Their concentrations rebounded during the post-lockdown period (e.g., more than twofold increase for Cu). Decreases were also observed in dust-related components (Ca, Ti, Mn; by 13-29%) when dust transport events were excluded, likely indicating reduced road-dust resuspension.

Mean diurnal cycles during the three periods are displayed in Fig. 1 for 13 elements. The metals most associated with non-exhaust vehicular emissions (Cu, Fe, Zn) generally displayed typical bimodal cycles, with peak concentrations during the morning rush hour (6:00 – 9:00) and in the evening (18:00-24:00) (Campbell et al., 2024). Cu was the one most closely linked (r: 0.59-0.70 for the full period, Fig. S7) to traffic-related variables (BC_{ff}, CO, NO_x) (Sofowote et al., 2019). The nighttime enhancement was more pronounced in the cold period, due to reduced MLH. While the morning peak persisted during the lockdown, the diurnal variability was less pronounced, particularly during the nighttime curfew (from 21:00 to the morning). The bimodality of Cu, a brake wear tracer, with rush-hour maxima, indicated the impact of acceleration-deceleration cycles under traffic congestion (Grigoratos and Martini, 2014). Evening increases in Zn were subtle (decreased emissions due to reduced speed variability, and limited resuspension of previously deposited tire wear particles under more humid nighttime conditions) (Amato et al., 2014; Müller et al., 2025). Cold-period K levels exhibited an elevated nocturnal plateau extending into the early morning (Fourtziou et al., 2017) and showed high correlations ($r > 0.75$) with BC_{bb}, BBOA, and LO-OOA (the latter closely related to the rapid processing of BB emissions under cold conditions) (Stavroulas et al., 2019). The maximum short-term K concentration during the cold period was slightly above 1 μg m^{-3}, still lower than values exceeding 5 μg m^{-3} during haze events in Chinese megacities (Liu et al., 2020; Yu et al., 2018). Although residential BB was not active for the entire lockdown period, it nevertheless affected the diurnal variability of K. The Ni cycle showed peaks in the morning (and in the evening during the warm period) that probably relate to departure/arrival times of passenger ships. Crustal elements exhibited clear daytime enhancements under summer conditions that favor resuspension. In colder conditions, the cycles displayed minor morning peaks (06:00-12:00; more pronounced

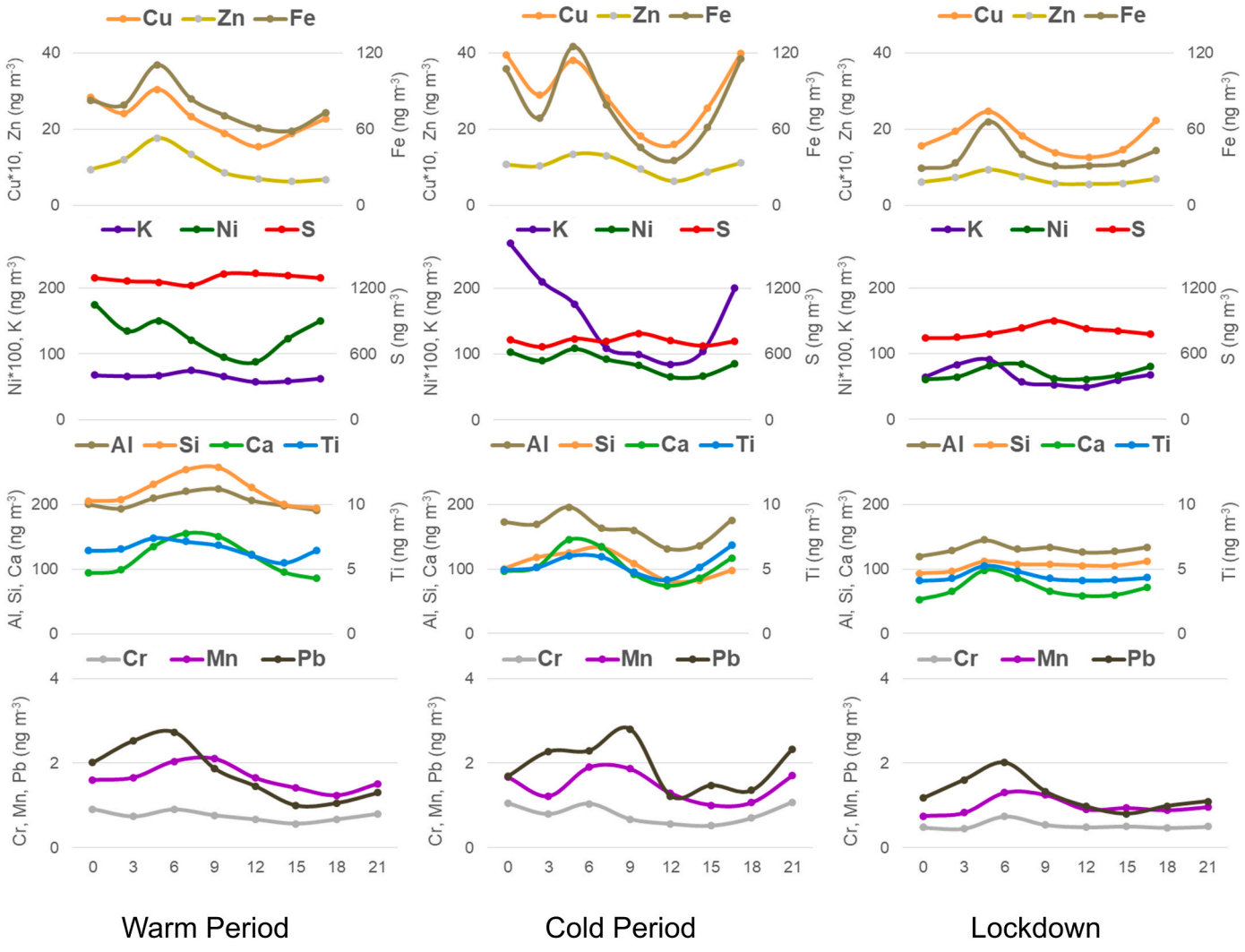

Fig. 1. Mean diurnal variability for 13 elements in $PM_{2.5}$, measured by the PX-375 analyzer during the three study periods (events related to wildfires, Saharan dust outbreaks, and fireworks were excluded).

for Ca), suggesting a potential impact from traffic-induced dust resuspension. The variation of Mn followed that of crustal elements, Cr showed a morning increase, and Pb exhibited more erratic variability (Ryder et al., 2020; Sofowote et al., 2019). Nonetheless, Pb recorded significant correlations (r: 0.55-0.63, Fig. S7) with Cu, Zn, and BC_{ff}, consistent with its presence in brake pads or in resuspended legacy-contaminated road dust (Argyraki and Kelepertzis, 2014; Campbell et al., 2024; Fussell et al., 2022).

Enrichment factors (EFs) for the elements, relative to the Earth's crustal composition (Wedepohl, 1995), were calculated using Si as the reference element (Visser et al., 2015; Yu et al., 2019). Mean EFs per period are shown in Fig. S8, and the diurnal variability (Tseng et al., 2022) is displayed in Fig. S9. Mn was classified among crustal elements with EFs <10, unlike Cr and Pb, for which EFs >40 indicate a substantial anthropogenic origin (Grivas et al., 2018). While the diurnal variability of typical crustal elements such as Al and Ti EFs was flat, Fe, Ca and Mn showed increases during morning traffic hours, similar to Cu and Zn, indicating an additional impact from non-exhaust emissions and road dust resuspension.

3.2. Episodic air quality events during the study periods

The online elemental data enabled a more in-depth study of episodes that can lead to exceedances of the new EU daily limit value for $PM_{2.5}$.

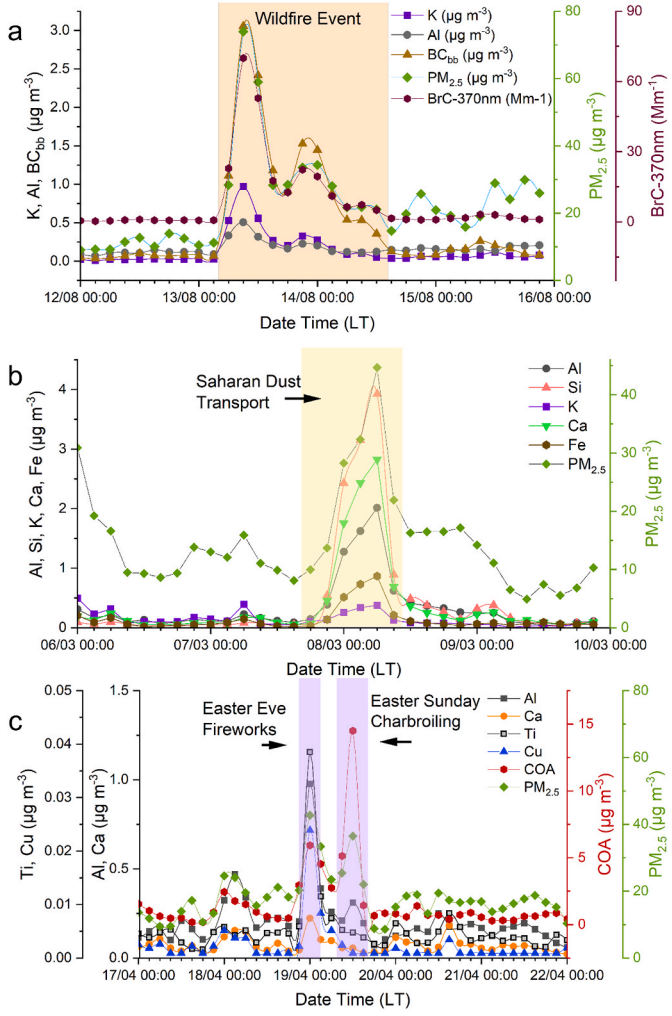

Fig. 2. Short-term variability of elemental concentrations and source-related aerosol components during air quality events (a: August 2019 Euboea wildfire; b: March 2020 Saharan dust outbreak; c: Fireworks and last-scale charbroiling during the orthodox Easter Weekend in 2020).

Fig. 2 presents three distinct events, one in each study period.

a) Wildfire smoke plume transport:

First, the large peri-urban wildfire of August 2019, which transported smoke from Euboea to the GAA (Fig. S10a), drove a substantial increase in $PM_{2.5}$ concentrations. $PM_{2.5}$ peaked at 74 μg m^{-3} on the morning of August 13 (9:00-12:00), closely associated with the rise in K concentrations (r = 0.93 over August 13-14) (Liu et al., 2018), which reached a warm-period maximum of 1.0 μg m^{-3}. BB-related components, such as BC_{bb} and BrC absorption in the near-UV, exhibited similar variability with K (r = 0.98 for BC_{bb} and r = 0.96 for BrC-370nm). Notably, during the wildfire event, BrC dominated fine aerosol absorption (>60% at 370 nm) (Chakrabarty et al., 2023; Kelesidis et al., 2025). Al and Ca (the more labile minerals in topsoil and ash) (Fajković et al., 2022; Pereira et al., 2012) also presented increased concentrations at the same time. This can be attributed to the mobilization and mixing of dust from the wildfire area within the smoke plume (Perron et al., 2022; Wagner et al., 2018), driven by pyroconvection that generates thermal updrafts (Giannaros et al., 2022; Menut et al., 2022). The event persisted throughout the day, resulting in an exceedance (43 μg m^{-3}) of the $PM_{2.5}$ daily limit (25 μg m^{-3}), and the following day was also close (24 μg m^{-3}). Wildfires are a recurring source of aerosol pollution in summer, as major urban, peri-urban, and regional fire events affected the Athens Basin again in the summers of 2020-2021 and 2023-2024 (Kaskaoutis et al., 2024).

b) Saharan dust transport:

Concentrations of crustal elements, combined with PM_c data, air mass back-trajectories, and satellite imagery, were used to flag long-range transported (LRT) dust events. A major Saharan outbreak, with dust transport from the Libyan Desert, occurred on March 7-8, 2020 (Fig. S10b), during the Mediterranean spring dust season (Cuevas-Agulló et al., 2024). $PM_{2.5}$ concentrations began to increase in the afternoon of March 7 (Fig. 2b), as dust was entrained downward and, after settling under reduced turbulence within the stable nocturnal boundary layer, peaked at 45 μg m^{-3} the following morning. Period-maxima for Al, Si, Ti, Fe and Ca were observed, with elemental ratios during the 12-h peak of the event (Si/Al: 1.81, Ti/Al: 0.04, Fe/Al: 0.41, Ca/Al: 1.35) presenting similarities to those determined for transported dust from the Libyan desert sampled at Mediterranean sites (Gini et al., 2022; Marconi et al., 2014). The higher Ca/Al ratio compared to values commonly reported for Saharan dust (Formenti et al., 2003) reflects the dominance of calcitic–dolomitic formations in the Libya-Egypt source regions (Boraiy et al., 2023). The daily-average $PM_{2.5}$ concentration on the event day was close to the limit value (24 μg m^{-3}), whereas five more exceedances were recorded in dust event days (March 29-30 and May 16-18).

c) Fireworks and charbroiling during Easter festivities:

Finally, it was possible to trace the impact of fireworks during Orthodox Easter Eve celebrations, when their use is extensive throughout the GAA by people gathering at every church. The intensity of this event during the lockdown year was maximized, since almost the entire population remained in the city due to travel restrictions. High concentrations of trace elements (Ti, Al, Cu, Ca, as well as Cr, Zn, Pb, and Mn) used as colorants in fireworks (Vecchi et al., 2008) peaked during 00:00-03:00 of Easter (April 19), given that the firework event starts exactly at midnight (Fig. 2c). The largest increases relative to the previous 24-h average were observed for Ti (8-fold) and Cu (10-fold), used in white/silver and blue fireworks, respectively. Among the more toxic elements, Cr and Pb showed 5-fold increases, whereas Ni (along with Fe) was not affected by the event (Fig. S11). While the rise in S concentrations was small (20%), ACSM-chloride increased 6-fold, likely due to the

formation of non-refractory colorants, such as copper chloride (Drewnick et al., 2006; Koch, 2015). The potassium enhancement should not be attributed entirely to its use as an oxidizer or in black powder (Tremper et al., 2018), since K and *m/z* 60 concentrations had already begun to increase before midnight, indicative of residential BB. $PM_{2.5}$ maximized at 43 μg m^{-3}, and its levels persisted until early morning (Rai et al., 2020), which is remarkable as the duration of these firework celebrations is very short (less than half an hour). This enhancement, combined with the very high OA concentrations at midday on Easter, due to GAA-wide open-air charbroiling (Stavroulas et al., 2024), led to a $PM_{2.5}$ exceedance of 25 μg m^{-3}, linked to long-established practices in Greece that are difficult to regulate.

3.3. Short-term fine aerosol source apportionment

The obtained PMF solution comprises eight factors related to exhaust and non-exhaust traffic (Traffic EXH, Traffic Non-EXH), biomass burning (BB), Oil Combustion, LRT Dust, Mixed Natural particles, Nitrate, and Regional processed aerosol. $PM_{2.5}$ mass was well reconstructed (observed-over-predicted regression r^2 and least-square regression slope of 0.87 and 0.99, respectively, for the constrained solution), with an unaccounted fraction of 2.6% (Table S3, Fig. S5). Solutions with 4-10 factors were assessed, and the 8-factor solution stabilized most of the assessed diagnostics. The minimum Q/Q_{EXP} was obtained for 8 factors, with a value close to unity (0.92), indicating reasonably calculated uncertainties and satisfactory model fit. Moreover, this solution also maximized the reconstruction r^2 and slope, produced low maximum individual column mean (IM) and standard deviation (IS), had normal standardized residuals for $PM_{2.5}$ with no values outside the [−3, 3] range, and a very low rate of samples with $Q/Q_{exp} > 3$ (1.4%). No swaps were recorded in the DISP analysis for any of the applied dQ_{max} thresholds in either the base or constrained (DISP dQ: 0.53%) solutions. The minimum-maximum DISP ranges for the key identifying species were low (in presentation order for the constrained solution: BC: ±9%, Cu: ±6%, *m/z* 60: ±10%, Ni: ±18%, Si: ±7%, Ca: ±15%, NO_3^-: ±23%, S: ±7%), verifying the rotational stability. The bootstrap analysis showed excellent factor re-mapping (base solution: 7/8 factors >99.5% and 1/8 > 90%; constrained solution: 6/8 factors 100% and 2/8 > 99.5%). The error evaluation indicated that the solution is resistant to rotational and random errors (Paatero et al., 2014) (Table S3, Fig. S5). Solutions with fewer factors were unstable across multiple runs, and in the 7-factor solution there was mixing between the Traffic EXH and Oil Combustion factors. The 9-factor solution was characterized by fragmentation of the Traffic-Non Exhaust source without an obvious physical interpretation. The 10-factor solution showed a large increase in Q/Qexp with DISP swaps appearing, and further fragmentation of the LRT dust factor (Table S3, Fig. S5). Most importantly, the 8-factor solution was physically interpretable regarding the characteristics of the study area, and all factors were successfully validated based on their temporal variability, comparison with reference source profiles, in-profile diagnostic ratios, correlations with source-specific external variables (including BC and OA components), and source origins identified through wind and trajectory analysis (Section S3). Finally, it is noted that the selected solution was based on a balanced representation of species measured by the different instruments, as assessed by instrument-specific mean absolute values of uncertainty-scaled residuals (Δe_{SC}) (Shukla et al., 2023; Slowik et al., 2010) (Section S3). The characteristics and verification of resolved factors are presented below.

- Vehicular Traffic sources: Separate sources representing exhaust (**Traffic EXH**) and non-exhaust (**Traffic Non-EXH**) traffic emissions were identified. As shown in the factor profiles (Fig. 3), the **Traffic-EXH** source was dominated by BC, with a lower contribution to OC (Su et al., 2020; Windell et al., 2024). The share of this factor to BC (67%) is comparable to the BC_{ff}/BC ratio in the dataset (75%) if the BC contribution from the oil combustion factor is also considered, and agrees with long-term BC_{ff}/BC observations at the same site for the examined months (Liakakou et al., 2020). The OA fraction (15%) was also comparable to the HOA/OA (12%) ratio in the dataset. The two carbonaceous components were linked with an in-profile OA/BC ratio of 1.4. Assuming an OA/OC analogy of 1.3 for traffic-related primary OA, as indicated by past measurements at Thissio (Florou et al., 2017), would produce an OC/BC ratio around 1.1, indicative of a mixed fleet profile with substantial contribution from HDV emissions (Pio et al., 2011). Minor contributions to directly emitted elements (Cu, Zn, Cr) were also detected, mainly originating from lubricants and engine wear (Cheung et al., 2010).

For the **Traffic Non-EXH** factor, the highest contributions were observed for elements typically associated with brake, tire, and mechanical wear (Cu, Fe, Zn, as well as Cr, Mn, Pb, Ca). All elements were

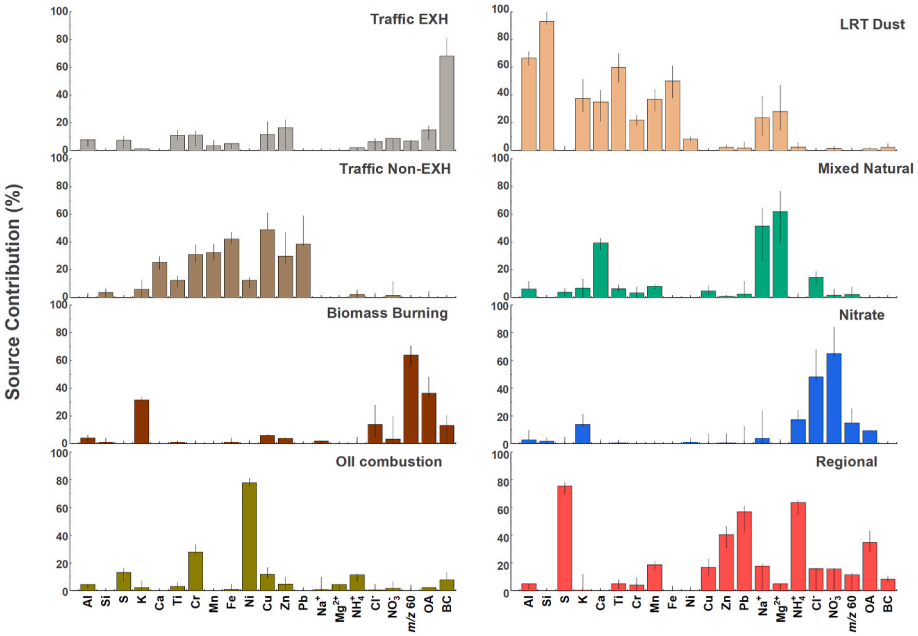

Fig. 3. PMF factor profiles (fractional factor contribution to species). Error bars indicate 5-95° BS intervals.

enriched with respect to crustal dust, with in-profile EFs exceeding 50. At the urban background site of the study, it was not possible to reliably separate brake and tire wear factors because they exhibit similar temporal profiles and dispersion dependence, while key elements (Cu, Fe, and Zn) contribute to both in varying degrees (Hicks et al., 2021). Moreover, they might partly originate from traffic-induced road dust resuspension (Amato et al., 2012; Hasheminassab et al., 2020). Cu/Fe and Zn/Fe ratios in the Traffic Non-EXH profile were used to assess the potential impact of road dust on the factor. Their values (0.03 and 0.08, respectively) were substantially higher than the ratios typically found in road dust particles (<0.01 for Cu/Fe, and <0.05 for Zn/Fe) (Huang et al., 2021; Skorbiłowicz et al., 2020). They were also comparable to ratios reported for mixed brake wear (0.03-0.07, with lower values associated with light-duty traffic; Charron et al., 2019) and tire wear emissions (0.05-0.15; Silva et al., 2021). The results indicate that the involvement of road dust resuspension in the factor is minor.

The exhaust factor consistently showed an excellent correlation (Fig. S12) with BC_{ff} ($r > 0.95$), and both traffic factors were associated with external variables related to vehicular circulation (CO, NO_x, CO_2) (Cheung et al., 2024; Manousakas et al., 2022; Shukla et al., 2023) across all periods. They also recorded the highest correlations with HOA (r: 0.51-0.86) among factors and showed the largest weekend reductions (23% combined reduction during the non-lockdown period, accentuated to 35% during the lockdown) (Fig. S13).

The diurnal cycles of both traffic-source $PM_{2.5}$ contributions (Fig. 4) showed morning rush-hour peaks and, during the cold period, became strongly bimodal under increased traffic. The morning peak was maintained during the lockdown (Sowlat et al., 2024), as vehicle circulation was not entirely prohibited, whereas the evening peak was suppressed by the curfew. On non-lockdown days, the diurnal cycles were similar between weekdays and weekends for both factors (Fig. S14), with a relative nocturnal enhancement on weekends, likely related to increased intra-city mobility for recreation (Hasheminassab et al., 2020; Kalkavouras et al., 2024). The polar plots (Uria-Tellaetxe and Carslaw, 2014)

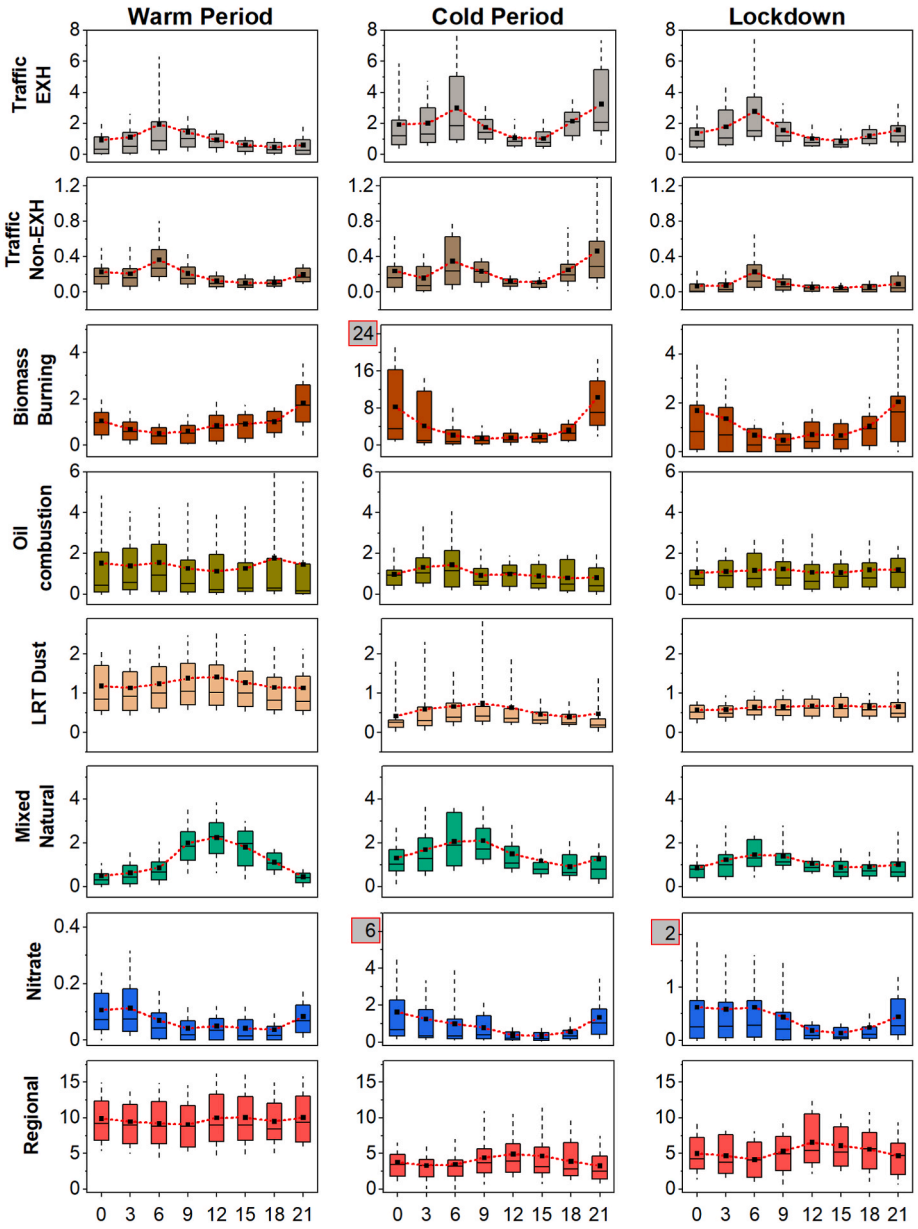

Fig. 4. Mean diurnal variation of PMF factor contributions (μg m^{-3}) at 3-h resolution for the three study periods (dot for the arithmetic mean, bar for the median, 25°-75° for the box, 10°-90° for the whiskers). Note the different scales in the shaded y-axis values. Events related to wildfires and severe Saharan dust outbreaks were excluded.

of both traffic factors showed enhancements under low wind speeds, attributable to circulation around local roads and the city's administrative center (Grivas et al., 2018) (Fig. S15). However, the annular plot for the exhaust source in Fig. S16 also indicated a daytime enhancement for winds from the SW, where commercial road transport is denser (Tsiodra et al., 2021). Moreover, the morning peak of the non-exhaust factor on lockdown weekends, when there was no go-to-work traffic, collapsed.

Therefore, while the two traffic factors were correlated, they presented differences, associated with the relative impacts of passenger cars (large number of gasoline cars, high road use) and commercial vehicles (including old vehicles and super-emitters) on non-exhaust and exhaust emissions, respectively (Grigoratos and Martini, 2014; Sokhi et al., 2022; Windell et al., 2024; Zhou et al., 2020). This distinction is consistent with prior results from Thissio, which showed that diesel vehicles contribute three times as much as gasoline cars to the carbonaceous content of tailpipe $PM_{2.5}$ (Tsiodra et al., 2021). Moreover, Jeong et al. (2022) in Toronto, Canada, observed lockdown-driven changes in the variability of exhaust and non-exhaust contributions similar to those observed here, and, using circulation data, linked the exhaust source to HDVs. Manousakas et al. (2022), apportioning $PM_{2.5}$ and $PM_{10\text{-}2.5}$ sources in Zurich, Switzerland, showed that non-exhaust emissions of fine PM are linked to light vehicles, as HDVs emit through brake and tire wear in the coarse fraction, and their fine elemental contributions come from tailpipe emissions. Shukla et al. (2023) in Delhi, India, also associated variability in Traffic-exhaust factor contributions with HDV circulation, regulated according to time-of-day restrictions (Tobler et al., 2020).

- Biomass Burning: The **BB** factor is mainly driven by residential heating emissions in the cold period (and partially in the lockdown), but also captures the effects of summer wildfire events. Even in the absence of the peak BB period (late December to January), the signal of the source was clear. The BB profile was characterized by the presence of the *m/z* 60 ACSM fragment (Faisal et al., 2025), serving as a proxy for levoglucosan, and by a substantial fraction of elemental K (32%; share offset by the presence of K in LRT dust) (Shukla et al., 2021). The source, despite its seasonal and essentially episodic character (whether in winter smog events or in wildfires), was one of the two largest contributors to fine OA during the study period (35%). The OA/BC ratio (assuming OA/OC: 1.5, again based on winter AMS measurements by Florou et al., 2017) was 10.9, close to the OC/EC values reported for PMF-resolved BB factors in Greece (Tsiodra et al., 2025). The high OA/BC ratio, combined with the factor contribution to OA, indicates that the BB-related OA in the present solution also includes rapidly processed organics, which in ACSM PMF appear as LO-OOA in the heating season (Stavroulas et al., 2019).

Consistent with this, the factor contributions showed the highest correlations (Fig. S12) not only with direct BB proxies (BC_{bb} and BBOA; *r*: 0.67-0.97) but also with LO-OOA (*r*: 0.77-0.85 during the lockdown and cold periods). Moreover, the source was associated with near-UV BrC absorption in all periods (*r*: 0.42-0.95), indicating its importance for the radiative budget at the urban/subregional scale (Paraskevopoulou et al., 2023). In contrast to traffic sources, the BB source presented a weekend enhancement related to recreational burning in fireplaces (Fig. S13) (Zhang et al., 2019a,b). The polar plot in Fig. S15 shows the effect of local emissions under stagnant conditions that induce smog events (Tsiodra et al., 2024).

As the short-term BB contributions to $PM_{2.5}$ during wildfire events reached 36 μg m^{-3} (≈65% of $PM_{2.5}$), these data were excluded from the assessment of the warm-period diurnal variations in Fig. 4. This is the first time that the diurnal variability of summer BB contributions has been assessed for $PM_{2.5}$ in Athens, and the results indicate a moderate increase from noon to midnight (Jeong et al., 2022; Stavroulas et al., 2024), which may be associated with wood-charcoal burning in meat charbroiling (Manousakas et al., 2022; Stavroulas et al., 2025). The results indicate that cooking organic aerosol, a substantial OA source in Athens, is probably classified in the BB source (also supported by BB-COA correlations; *r*: 0.70-0.88). Cooking aerosol was not isolated due to the lack of online-measured chemical tracers, a methodological limitation of the current approach. However, the combined contribution of BBOA, COA, and heating-season LO-OOA to OA was 33%, which is close to the full-period BB contribution estimated in the present PMF approach (36%). The warm-period concentrations can also be associated with long-range transport of BB emissions from intense summer agricultural burning in the Balkans and Eastern Europe (Vasilakopoulou et al., 2023), as indicated by the PSCF back-trajectory analysis (Fig. S18) (Petit et al., 2017). During the cold period, a U-shaped diurnal pattern was observed (Fig. 4) (Belis et al., 2019; Windell et al., 2024). Average nighttime (18:00-06:00) concentrations exceeding 6 μg m^{-3} were recorded, corresponding to a fractional contribution of 30% (Fig. S19), comparable to the share of the BB source reported during haze episodes in Chinese megacities (Liu et al., 2019a). In the lockdown, when residential BB was still active, it also contributed during the day (midday hump in Fig. S14, especially on weekends), reflecting increased indoor stay.

- Oil combustion related to shipping: The factor was attributed to Heavy Fuel **Oil Combustion**, given the strong presence of nickel (81%) (Chang et al., 2018). The source profile was compared with a composite marine fuel oil profile from the SPECIATE database (Simon et al., 2010) (Section S3), yielding good agreement ($r = 0.87$, SID = 0.65; $n = 10$). A significant correlation with SO_2 was also observed in the 2019 warm period ($r = 0.46$) (Jang et al., 2023). The factor was also associated with V (*r*: 0.60, full period) when used as an external indicator (given the good correlation of $V_{PX\text{-}375}$ with filter-based V, despite the large underestimation that led to its exclusion from PMF). The wind analysis results clearly link the factor to shipping emissions originating in the wider Piraeus Port area and to the corresponding navigation lanes to the S-SW (Fig. S15 and 16) (Grivas et al., 2018; Theodosi et al., 2018). This source area, which ties the factor to port and shipping activity, was consistently verified by Conditional Probability Function (CPF) plots across all study periods, and was also observed in independent CPF plots for Ni and V (Fig. S17). It is noted that there are no major stationary heavy oil combustion facilities in the Athens basin (Grivas et al., 2018), while advections from the Thriassion plain to the W-NW (where there are some large combustion plants) to central Athens are infrequent (Kassomenos et al., 1998).

The results in Fig. 4 provide first-time insights into the diurnal patterns of shipping-source contributions to $PM_{2.5}$ in Athens. Since operations at the commercial port of Piraeus are continuous, emissions from cargo ship navigation may be considered a baseline, potentially accounting for more than half of the total on average. This was evident during the lockdown, when the diurnal cycle was largely flat due to restrictions on passenger ship traffic (Fig. 4, Fig. S14). However, some variability remained on lockdown weekends, which might reflect ferry traffic transporting essential supplies, although this is difficult to assess (large increases were observed on specific weekends, such as those of the Easter period and the last weekend of the lockdown). Uniform diurnal variability in commercial shipping contributions was also reported in Shenzhen, China (Su et al., 2020). During the cold period in Athens, there was a peak in the early morning hours (06:00-09:00), coinciding with passenger ship departures from Piraeus for the Aegean islands. This effect was more pronounced during the warm period, when an additional increase over the baseline was observed in the evening (18:00-00:00), likely attributable to ferry arrivals and cruise ship departures in the late afternoon. It is noteworthy that evening peaks were not observed after August 20, when passenger activity at the port began to decline. The warm-period diurnal patterns are comparable to the diurnal variation of a shipping-related HOA factor derived from PMF on ACSM measurements at the Piraeus passenger port in June-July 2019 (Stavroulas et al., 2021). Moreover, a similar bimodal summer diurnal cycle was reported by a relevant two-step online PMF study in Marseille, France (Camman et al., 2024), one of the largest passenger ports in the

Mediterranean (Le Berre et al., 2025).

- Natural sources: Two factors related to the contribution of natural sources to fine particles were identified. The factor named **LRT Dust** was represented by crustal species (Al, Si, Ca, Fe, Ti, Mn). All elements in the profiles had EFs <3. The almost exclusive association of the factor with winds from the southern sector is evident in Fig. S15. Moreover, the PSCF analysis highlighted that the highest contributions were linked to transport from the Libyan Desert, which is frequent during the dust season (Kalivitis et al., 2007) (Fig. S18). The correlations of the factor with PMc were significant year-round ($r > 0.40$), even with the exclusion of major dust events. During the cold period, the March 7-8 episode (Section 3.2) led to 3-hr contributions to $PM_{2.5}$ exceeding 60%. On non-event days, the source exhibited limited diurnal variability across all periods, whereas the effects of sustained LRT dust activity in March were reflected by the high-percentile increases (Fig. 4).

The **Mixed Natural** factor represents locally resuspended soil particles and sea salt. Its profile was characterized by the presence of Na^+ and Mg^{2+} ions, as well as Ca (with an in-profile EF of 7). The high abundance of Ca compared to seawater indicates the impact of local dust resuspension under favorable weather conditions. The soil in Athens is characterized by a pronounced carbonate signature, dominated by calcite. As a result, Ca in fine dust is decoupled from the aluminosilicate minerals of the previous factor. The in-profile Al/Ca, K/Ca and Mn/Ca ratios were very close to the values reported for the mean geochemical profile of the GAA (Argyraki and Kelepertzis, 2014). Increased wind-induced resuspension from dry surfaces in summer is a driving factor (Camman et al., 2024; Yu et al., 2019), and significant correlations with temperature and wind speed ($r \approx 0.4$) were recorded. High factor contributions were associated with strong winds that induced local resuspension and upslope transport of calcite-rich dust to the site, along with marine aerosol transport (Fig. S15). As such winds are more frequent during the day (Section 2.1.1), there were enhancements in the 6:00-12:00 interval in all periods (Fig. 4) (Fourtziou et al., 2017), and in the summer they extended up to 18:00 under the effect of pure sea-breeze and strong Etesian winds. The diurnal variability (Fig. 4) might also suggest that road dust resuspension affects this factor. Although all correlations with traffic proxies were weak, dust resuspension has been reported not to scale with traffic volume (Hicks et al., 2021). A mixed soil/sea-salt factor was also identified using high-resolution, dispersion-normalized PMF at an inland site in Tianjin, China (Dai et al., 2020), with comparable diurnal variation and wind dependence. The same diurnal/seasonal patterns were also reported for a local soil resuspension source in Los Angeles, CA, by the long-term study of Hasheminassab et al. (2020). The distinction between episodic LRT and local mineral dust has also been made through online XRF source apportionment in Zurich, with the latter exhibiting a wind-induced midday enhancement (Manousakas et al., 2022).

- Secondary Aerosol: Two factors related to the regional and local formation of secondary aerosol were quantified. The first, distinguished by the presence of **Nitrate**, is associated with the local formation of secondary aerosol. Non-refractory chloride was classified here, along with a minor fraction of K. The factor was almost exclusively observed during cold/lockdown periods and was linked to nighttime processing of BB emissions (Jorga et al., 2021). Large NO_x amounts are produced by residential BB, promoting nighttime NO_z chemistry, while BB aerosol provides increased surface area for the heterogeneous formation of nitric acid (Goldberger et al., 2019; Jorga et al., 2021; Kukkonen et al., 2020). These reactions are rapid enough that BB marker and nitrate levels peak concurrently during winters in the GAA (Stavroulas et al., 2021). Chloride is also present in biomass and can be co-emitted as HCl, which then partitions into the particle phase under favorable temperature and acidity conditions on winter nights (Shukla et al., 2025). Consequently, the factor was strongly correlated with BC_{bb}, BBOA, and LO-OOA ($r > 0.65$; Fig. S12) during the cold and lockdown periods (Stavroulas et al., 2019, 2024).

The second processed factor was dominated by non-refractory ammonium sulfate and was named **Regional**, in accordance with past studies at Thissio (Theodosi et al., 2018; Tsiodra et al., 2024). The factor represents particles transported to the receptor after atmospheric processing of their anthropogenic precursors, primarily from power production and industrial activity. Therefore, elements such as Pb and Zn, which are co-emitted with SO_x by coal- and oil-burning in distant locations (Rai et al., 2020), contribute to the profile in addition to sulfate. The presence of strongly processed secondary organic aerosol was indicated by the high OA/BC ratio (assuming an OA/OC ratio of 2, this would yield OC/BC ≈ 12). Therefore, high year-round correlations with MO-OOA were registered ($r > 0.65$; Fig. S12), and the factor's contribution to OA (32%) was directly comparable to the ACSM-based MO-OOA/OA ratio. The origin of this regionally processed aerosol can be traced back to the Balkans, the Black Sea Region, Ukraine, and Southern Russia (Fig. S18) (Argyropoulos et al., 2017; Dimitriou et al., 2023). The diurnal variability (Fig. 4) was limited (Shukla et al., 2021, 2025), similar to that of the other LRT factor (Dust), with small early-afternoon increases, typically for sulfate and SOA under increased vertical mixing in the expanded boundary layer (Yu et al., 2019).

3.4. Source contributions to $PM_{2.5}$

Fig. 5 presents the mean source contributions (fractional and net) across the three study periods. Traffic-exhaust emissions during 2019-2020 appeared to be the more effective of the two vehicular components for the urban background of central Athens, as the mean contribution of non-exhaust particles did not exceed 0.5 μg m^{-3}. The same pattern among the two components has been observed in filter-based PMF studies in Athens during 2013-2017 (Diapouli et al., 2022; Manousakas et al., 2021). However, their relative shares at the European level can vary substantially (Amato et al., 2016; Saraga et al., 2021). These contributions in Athens should be reassessed in light of the gradual modernization of the car and truck fleet, the growth in car ownership, and the increasing number of hybrid/electric vehicles (Spyropoulos et al., 2022; Timmers and Achten, 2016).

Consistent with past studies at Thissio on various aerosol metrics (e.g., Stavroulas et al., 2019; Tsiodra et al., 2021), the still-unregulated BB source dominated during the cold season (27%, 34% when secondary nitrate was included), even though there were no measurements from the peak residential heating period (meaning that the actual BB contribution on an annual basis should be higher). The oil combustion source (shipping) contributed 7-9% on average, which is reasonable considering the pre-2020 range reported by the review study of Sorte et al. (2020) for coastal areas in the Mediterranean, but lower than those estimated for Thissio in 2014-2015 (1.1-1.5 vs. 1.7 μg $^{-3}$) (Theodosi et al., 2018). The importance of passenger shipping was reflected in the significant warm vs. cold period enhancement of the source contribution (0.4 μg m^{-3}, +38%), even though the winter baseline remained substantial (0.7 μg m^{-3}; Fig. 4). These results were obtained during the transition to the 2020 IMO sulfur cap of 0.5%, which, combined with the declaration of the Mediterranean as a SECA, is expected to further reduce shipping emissions (Eiof Jonson et al., 2020; Toscano, 2023). The two natural particle factors contributed a substantial background of 2.6 μg m^{-3} (16%), in a year with major dust events. Saharan dust transport in the Mediterranean is sustained for a large part of spring-summer, with the frequency of dust days reaching 20%. However, the absence of the early winter period in the dataset, when LRT events are less frequent, should be noted (Vogel et al., 2025). The mean LRT dust concentration of 1.2 μg m^{-3} is comparable to the annual average LRT contribution to $PM_{2.5}$ (1.5 μg m^{-3}, 14%) reported over Athens in 2014 (Diapouli et al., 2017). This natural background, combined with the contribution of regionally processed aerosol, which partly originates from countries not bound by EU emission legislation, poses barriers to future compliance with the EU standard (Im et al., 2012). The regional factor showed a warm-period enhancement, accounting for more than half of the $PM_{2.5}$ mass. Its winter contribution

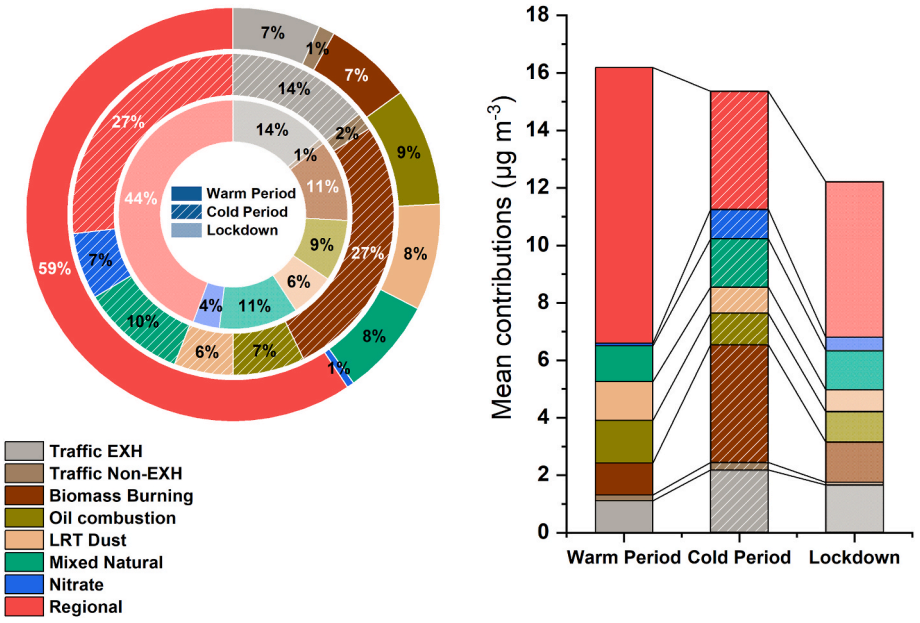

Fig. 5. Fractional (left) and net (right) contributions of PMF-resolved factors to $PM_{2.5}$ concentrations over the warm, cold, and lockdown periods of the study.

(27%) was comparable to that reported by a multi-year (2013-2016) study at Thissio (Theodosi et al., 2018), but smaller in magnitude (4.1 μg m^{-3} vs. 4.7 μg m^{-3}), while the higher summer-mean reflects the enhanced processing of SO_x and organic precursors.

The moderate reduction in $PM_{2.5}$ during the lockdown (−15% relative to the cold-period mean) has been documented by Grivas et al. (2020), and here it was possible to attribute it to specific sources. Both traffic factors presented decreases (by 0.4 and 0.2 μg m^{-3} for Traffic-EXH and Traffic Non-EXH, respectively). The combined fractional decrease for the traffic sources was 29% (Hicks et al., 2021), slightly lower than reductions for traffic-related parameters (e.g., 35% for BC_{ff} and 34% for CO). It is noted that the decline in passenger traffic during the lockdown was far greater than that of commercial vehicles (Schulte-Fischedick et al., 2021). In this sense, a higher reduction rate for non-exhaust than for exhaust emissions (64% vs. 20%) is consistent with the pattern discussed in Section 3.3, in which the former are primarily driven by passenger-car volume (Sofowote et al., 2019). Traffic source contributions rebounded immediately after the lockdown, with increases of 1.6 and 0.4 μg m^{-3} in the post-lockdown week (Sowlat et al., 2024). A large lockdown reduction (−64%) was also observed for the BB and nitrate factors, as the effect of residential heating diminished from early April onward. The decline in local primary sources was partially offset by increased contributions from regional aerosols, as favorable conditions for secondary formation overcame the COVID-related decrease of precursor emissions (Jeong et al., 2022). Although the lockdown decrease in the oil combustion source was not significant, the large post-lockdown increase (1.4 μg m^{-3}) likely reflects the resumption of passenger shipping activity following the restrictions.

3.5. *Diurnal variability of potential risks from exposure to elemental concentrations*

Fig. 6 displays the diurnal variation of fractional factor contributions to the non-carcinogenic ($\sum_i C_i/RfC_i$) risk indicator along with its cumulative value (Section 2.5). Results for the carcinogenic risk indicator are shown in Fig. S20. The analysis misses some elements with important RfC and IUR values, such as Cd (not quantified by the PX-375 monitor), and As-V (severely underestimated and excluded from source apportionment). Even if As and V were included in the PMF analysis (which would, in turn, lead to their uncertain apportionment

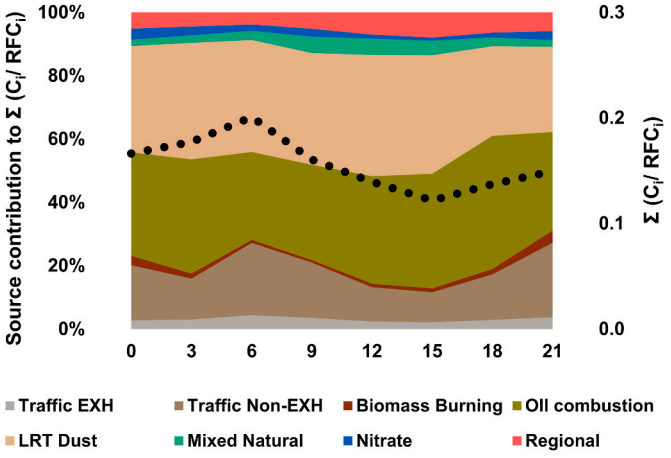

Fig. 6. On the left axis, diurnal variation of the fractional factor contributions (colored areas) to the non-carcinogenic risk indicator. The diurnal variation of the indicator (dotted line) is shown on the right axis.

and mass reconstruction), the results presented below would not be substantially modified due to their very low concentrations.

As can be observed from the average values of the indicators (Fig. 6, Fig. S20), the acceptable thresholds for non-carcinogenic and carcinogenic risk (1 and 10^{-6}, respectively) would not have been exceeded if they had been scaled using nominal exposure-time parameters. This is typical in European cities where large point sources of toxic metals are sparse (Chalvatzaki et al., 2019; Galindo et al., 2018). However, the analysis provides insights into the diurnal patterns of systemic toxicity from exposure to ambient metals and the relative contributions of their sources. The total values of both risk indicators peaked during the morning commute hours and formed a nighttime plateau when outdoor population exposure is typically minimal.

The diurnal variability was driven by the two traffic components (contributing 20% and 50% to non-carcinogenic and carcinogenic risk, respectively) (Lakra et al., 2026). Traffic-related risks peak during the morning hours when a large share of the population is most exposed to traffic emissions (Assimakopoulos et al., 2018). Traffic is also a significant driver of OP in Athens (Paraskevopoulou et al., 2019), and the

non-exhaust source was the largest contributor to redox-active transition metals. The contributions of BB were small for both risk types; however, BB emissions in Athens have been strongly associated with non-acceptable carcinogenic risks from inhalation exposure to polycyclic aromatic compounds (Tsiodra et al., 2024). Moreover, as stated in Section 3.4, the long-term BB contribution is expected to be somewhat underestimated because data from the peak residential burning period were not available for the analysis. Despite its small share in $PM_{2.5}$, the oil combustion source contributed significantly to both indicators (33-34%) in the present dataset due to its association with Ni and Cr (Wen et al., 2018). The importance of the shipping source for non-carcinogenic $PM_{2.5}$ toxicity was also demonstrated in Xiamen, China (Wu et al., 2020). The contribution of the regional factor was small, although it would be increased by the inclusion of toxic and carcinogenic As and Cd, which have been associated with regional transport of emissions from large point sources (Pandolfi et al., 2016).

4. Conclusions

Seasonal patterns and diurnal variations in the elemental composition of fine particulate matter and related source contributions were investigated through intensive monitoring campaigns, under conditions representative of the urban background in central Athens, Greece. Online measurements were performed in central Athens across warm, cold, and lockdown periods in 2019-2020. The $PM_{2.5}$ composition for 15 elements was determined at a 3-h resolution using the Horiba PX-375 EDXRF analyzer. The bulk fine-aerosol composition (carbonaceous compounds and major ions) was concurrently monitored. Results obtained with the PX-375 were meaningful for short-term temporal variability, and the concentration levels for most elements (except As and V) were comparable and well correlated with those determined by filter-based ICP-MS. However, the absence of certain tracer elements in the instrument version used imposed certain limitations on the source characterization. This was evident for the sea-salt elements, here determined by online PILS ion chromatography (a resource-intensive method), whose inclusion did not result in the isolation of a sea-salt factor.

The speciated data were processed within a combined receptor modeling framework, based on single combined PMF. This PMF approach explored the possibility of obtaining environmentally meaningful results by applying receptor modelling to the bulk chemical composition measured by online instruments. There were some caveats in its implementation, mostly related to uncertainty calculations (not instrument-provided by the PX-375) and to merging monitors of fine aerosols with different size distributions. Moreover, despite the extended temporal coverage of concurrent multi-instrument measurements, data were unavailable during the peak residential heating period (December–January), which may introduce bias when inferring long-term concentrations and exposures, particularly for biomass-burning aerosols. However, the results provided insights into contribution levels and variability across a broad range of fine aerosol sources, suggesting that similar studies, but on a long-term basis, will be valuable for policy and exposure management. For the first time, it was possible to assess the effects of the 2020 COVID-19 lockdown on $PM_{2.5}$ sources in Athens, indicating moderate reductions in local sources but not in regional anthropogenic aerosols.

In 2020, traffic remained a substantial $PM_{2.5}$ source in urban background areas of Athens (8-16% seasonally). Despite emission regulations over the last decade, persistent levels reflect the age of the vehicular fleet and the circulation of heavy emitters. The non-exhaust component accounted for a lower share of the combined vehicular source (12%). Still, its bearing in elemental toxicity assessments might be increased due to its association with toxic and redox-active transition elements. The diurnal patterns during the lockdown for traffic-related factors imply that achieving significant reductions in $PM_{2.5}$ from traffic in urban background areas would necessitate drastic cuts in road transport emissions. The Oil Combustion source, closely associated with shipping emissions in the Piraeus port area, contributed 7-9% to $PM_{2.5}$ at inland locations, with diurnal variability apparently affected by passenger shipping, indicating a source effect that probably extends beyond ports and coastal areas. These shipping impacts need to be reevaluated in the context of the 2020 IMO global sulfur cap and the declaration of the Mediterranean as a Sulfur Emission Control Area (SECA) in 2025, while also considering that apportioning the source will become more difficult in an era of very low-sulfur oil and alternative marine fuels. The staggering impact of residential BB during the cold period in Athens was reaffirmed, with the source impact extending into the spring lockdown period due to increased recreational BB associated with greater time spent indoors. However, the results from the high-resolution measurements also underscore the need to assess more rigorously the BB effects in summer, when less-intense local emissions are augmented by distant agricultural burning and peri-urban wildfires.

The period-mean $PM_{2.5}$ source contributions and the baselines derived from their diurnal variations imply significant challenges in attaining the new EU long-term limit value in the GAA. Natural and LRT aerosols constitute a substantial background, rendering threshold attainment largely contingent on mitigating urban aerosol emissions. The relative impact of the sources contributing to this baseline in the region needs to be gauged under true background conditions that limit interference from local sources. Moreover, in a study period not including the December-January period, when numerous BB smog events are consistently observed, there were 12 exceedances of the new EU daily limit value, eight of which were due to episodic events of recurring nature, not possible to control. Therefore, violations of the short-term standard are probable in urban background areas in Athens, and even more at polluted sites. Thus, this research should be replicated in high-exposure settings, such as roadside and near-port locations.

Funding

This research was funded by the National Observatory of Athens internal grant "ERSILIA - Enhanced-Resolution Source Identification for aerosoL In Athens" (project no. 5086).

CRediT authorship contribution statement

Georgios Grivas: Conceptualization, Data curation, Formal analysis, Funding acquisition, Investigation, Methodology, Project administration, Validation, Visualization, Writing – original draft, Writing – review & editing. **Eleni Liakakou:** Data curation, Investigation, Writing – review & editing. **Panayiotis Kalkavouras:** Investigation, Writing – review & editing. **Iasonas Stavroulas:** Investigation, Writing – review & editing. **Kalliopi Petrinoli:** Data curation. **Despina Paraskevopoulou:** Data curation. **Irini Tsiodra:** Visualization. **Maria Tsagkaraki:** Data curation. **Aikaterini Bougiatioti:** Data curation. **Alessandro Bigi:** Methodology. **Evangelos Gerasopoulos:** Funding acquisition. **Nikolaos Mihalopoulos:** Resources, Supervision, Writing – review & editing.

Declaration of competing interest

The authors declare that they have no known competing financial interests or personal relationships that could have appeared to influence the work reported in this paper.

Acknowledgements

We acknowledge support for this work by the project "PANhellenic infrastructure for Atmospheric Composition and climatE change" (MIS 5021516), which is implemented under the Action "Reinforcement of the Research and Innovation Infrastructure", funded by the Operational Programme "Competitiveness, Entrepreneurship and Innovation" (NSRF 2014–2020) and co-financed by Greece and the European Union

(European Regional Development Fund). We thank Horiba Inc. and Envirosys Ltd. for providing the PX-375 online metals analyzer during the campaigns, and especially Patrice Moubea from HORIBA Europe GmbH for supporting the installation and providing training on the instrument. The research personnel of the ECPL laboratory of the University of Crete are acknowledged for performing filter-based aerosol composition analyses.

Appendix A. Supplementary data

Supplementary data to this article can be found online at https://doi.org/10.1016/j.atmosenv.2026.122061.

Data availability

Data will be made available on request.

References

Aguilera, R., Corringham, T., Gershunov, A., Benmarhnia, T., 2021. Wildfire smoke impacts respiratory health more than fine particles from other sources: observational evidence from Southern California. Nat. Commun. 12. https://doi.org/10.1038/S41467-021-21708-0.

Ahmad, M., Thaveevong, P., Aman, N., Ngamsritrakul, T., Panyametheekul, S., 2025. The $PM_{2.5}$-bound metals in the metropolitan area of Bangkok, Thailand: temporal trends, sources, and human health challenges. Environ. Chall. 18, 101092. https://doi.org/10.1016/J.ENVC.2025.101092.

Amato, F., Alastuey, A., De La Rosa, J., Sánchez De La Campa, A.M., Pandolfi, M., Lozano, A., Contreras González, J., Querol, X., 2014. Trends of road dust emissions contributions on ambient air particulate levels at rural, urban and industrial sites in southern Spain. Atmos. Chem. Phys. 14, 3533–3544. https://doi.org/10.5194/ACP-14-3533-2014.

Amato, F., Alastuey, A., Karanasiou, A., Lucarelli, F., Nava, S., Calzolai, G., Severi, M., Becagli, S., Gianelle, V.L., Colombi, C., Alves, C., Custódio, D., Nunes, T., Cerqueira, M., Pio, C., Eleftheriadis, K., Diapouli, E., Reche, C., Minguillón, M.C., Manousakas, M.I., Maggos, T., Vratolis, S., Harrison, R.M., Querol, X., 2016. AIRUSE-LIFE+: a harmonized PM speciation and source apportionment in five southern European cities. Atmos. Chem. Phys. 16, 3289–3309. https://doi.org/10.5194/ACP-16-3289-2016.

Amato, F., Karanasiou, A., Moreno, T., Alastuey, A., Orza, J.A.G., Lumbreras, J., Borge, R., Boldo, E., Linares, C., Querol, X., 2012. Emission factors from road dust resuspension in a Mediterranean freeway. Atmos. Environ. 61, 580–587. https://doi.org/10.1016/J.ATMOSENV.2012.07.065.

Argyraki, A., Kelepertzis, E., 2014. Urban soil geochemistry in Athens, Greece: the importance of local geology in controlling the distribution of potentially harmful trace elements. Sci. Total Environ. 482–483, 366–377. https://doi.org/10.1016/J.SCITOTENV.2014.02.133.

Argyropoulos, G., Samara, C., Diapouli, E., Eleftheriadis, K., Papaoikonomou, K., Kungolos, A., 2017. Source apportionment of PM_{10} and $PM_{2.5}$ in major urban Greek agglomerations using a hybrid source-receptor modeling process. Sci. Total Environ. 601–602, 906–917. https://doi.org/10.1016/j.scitotenv.2017.05.088.

Asano, H., Aoyama, T., Mizuno, Y., Shiraishi, Y., 2017. Highly time-resolved atmospheric observations using a continuous fine particulate matter and element monitor. ACS Earth Space Chem. 1, 580–590. https://doi.org/10.1021/ACSEARTHSPACECHEM.7B00090.

Assimakopoulos, V.D., Bekiari, T., Pateraki, S., Maggos, T., Stamatis, P., Nicolopoulou, P., Assimakopoulos, M.N., 2018. Assessing personal exposure to PM using data from an integrated indoor-outdoor experiment in Athens-Greece. Sci. Total Environ. 636, 1303–1320. https://doi.org/10.1016/J.SCITOTENV.2018.04.249.

Belis, C.A., Pikridas, M., Lucarelli, F., Petralia, E., Cavalli, F., Calzolai, G., Berico, M., Sciare, J., 2019. Source apportionment of fine PM by combining high time resolution organic and inorganic chemical composition datasets. Atmos. Environ. X, 100046. https://doi.org/10.1016/J.AEAOA.2019.100046.

Bhowmik, H.S., Shukla, A., Lalchandani, V., Dave, J., Rastogi, N., Kumar, M., Singh, V., Tripathi, S.N., 2022. Inter-comparison of online and offline methods for measuring ambient heavy and trace elements and water-soluble inorganic ions (NO_3^-, SO_4^{2-}, NH_4^+, and Cl^-) in $PM_{2.5}$ over a heavily polluted megacity, Delhi. Atmos. Meas. Tech. 15, 2667–2684. https://doi.org/10.5194/amt-15-2667-2022.

Bi, X., Zhang, G., Li, L., Wang, X., Li, M., Sheng, G., Fu, J., Zhou, Z., 2011. Mixing state of biomass burning particles by single particle aerosol mass spectrometer in the urban area of PRD, China. Atmos. Environ. 45, 3447–3453. https://doi.org/10.1016/J.ATMOSENV.2011.03.034.

Boraiy, M., El-Metwally, M., Borbon, A., Chevaillier, S., Laurent, B., Lafon, S., El Sanabary, F.F., Masmoudi, M., Alfaro, S.C., 2023. Elemental ratios as tracers of the sources of mineral dust in north-eastern Sahara. Int. J. Environ. Sci. Technol. 212 21, 1875–1888. https://doi.org/10.1007/S13762-023-05077-3, 2023.

Briggs, N.L., Long, C.M., 2016. Critical review of black carbon and elemental carbon source apportionment in Europe and the United States. Atmos. Environ. 144, 409–427. https://doi.org/10.1016/j.atmosenv.2016.09.002.

Brown, S.G., Eberly, S., Paatero, P., Norris, G.A., 2015. Methods for estimating uncertainty in PMF solutions: examples with ambient air and water quality data and guidance on reporting PMF results. Sci. Total Environ. 518–519, 626–635. https://doi.org/10.1016/J.SCITOTENV.2015.01.022.

Buset, K.C., Evans, G.J., Richard Leaitch, W., Brook, J.R., Toom-Sauntry, D., 2006. Use of advanced receptor modelling for analysis of an intensive 5-week aerosol sampling campaign. Atmos. Environ. 40, 482–499. https://doi.org/10.1016/J.ATMOSENV.2005.12.074.

Camman, J., Chazeau, B., Marchand, N., Durand, A., Gille, G., Lanzi, L., Jaffrezo, J.L., Wortham, H., Uzu, G., 2024. Oxidative potential apportionment of atmospheric PM_1: a new approach combining high-sensitive online analysers for chemical composition and offline OP measurement technique. Atmos. Chem. Phys. 24, 3257–3278. https://doi.org/10.5194/ACP-24-3257-2024.

Campbell, S.J., Barth, A., Chen, G.I., Tremper, A.H., Priestman, M., Ek, D., Gu, S., Kelly, F.J., Kalberer, M., Green, D.C., 2024. High time resolution quantification of $PM_{2.5}$ oxidative potential at a Central London roadside supersite. Environ. Int. 193, 109102. https://doi.org/10.1016/j.envint.2024.109102.

Canonaco, F., Crippa, M., Slowik, J.G., Baltensperger, U., Prévôt, A.S.H., 2013. SoFi, an IGOR-based interface for the efficient use of the generalized multilinear engine (ME-2) for the source apportionment: ME-2 application to aerosol mass spectrometer data. Atmos. Meas. Tech. 6, 3649–3661. https://doi.org/10.5194/AMT-6-3649-2013.

Canonaco, F., Tobler, A., Chen, G., Sosedova, Y., Gates Slowik, J., Bozzetti, C., Rudolf Daellenbach, K., El Haddad, I., Crippa, M., Huang, R.J., Furger, M., Baltensperger, U., Prévôt, A.S.H., 2021. A new method for long-term source apportionment with time-dependent factor profiles and uncertainty assessment using SoFi Pro: application to 1 year of organic aerosol data. Atmos. Meas. Tech. 14, 923–943. https://doi.org/10.5194/AMT-14-923-2021.

Chakrabarty, R.K., Shetty, N.J., Thind, A.S., Beeler, P., Sumlin, B.J., Zhang, C., Liu, P., Idrobo, J.C., Adachi, K., Wagner, N.L., Schwarz, J.P., Ahern, A., Sedlacek, A.J., Lambe, A., Daube, C., Lyu, M., Liu, C., Herndon, S., Onasch, T.B., Mishra, R., 2023. Shortwave absorption by wildfire smoke dominated by dark brown carbon. Nat. Geosci. 168 (16), 683–688. https://doi.org/10.1038/s41561-023-01237-9, 2023.

Chalvatzaki, E., Chatoutsidou, S.E., Lehtomäki, H., Almeida, S.M., Eleftheriadis, K., Hänninen, O., Lazaridis, M., 2019. Characterization of human health risks from particulate air pollution in selected European cities. Atmosphere 10. https://doi.org/10.3390/ATMOS10020096, 2019 Page 96 10, 96.

Chang, Y., Huang, K., Xie, M., Deng, C., Zou, Z., Liu, S., Zhang, Y., 2018. First long-term and near real-time measurement of trace elements in China's urban atmosphere: temporal variability, source apportionment and precipitation effect. Atmos. Chem. Phys. 18, 11793–11812. https://doi.org/10.5194/acp-18-11793-2018.

Charron, A., Polo-Rehn, L., Besombes, J.L., Golly, B., Buisson, C., Chanut, H., Marchand, N., Guillaud, G., Jaffrezo, J.L., 2019. Identification and quantification of particulate tracers of exhaust and non-exhaust vehicle emissions. Atmos. Chem. Phys. 19, 5187–5207. https://doi.org/10.5194/acp-19-5187-2019.

Chasapi, M.-A., Moustris, K., Fameli, K.-M., Spyropoulos, G., 2025. The application of an empirical method for the estimation of vehicles' contribution to air pollution in an urban environment: a case study in Athens, Greece. Air Water Pollut. Rep. 3, 14. https://doi.org/10.3390/AIR3020014, 2025.

Chen, H., Zhang, Z., Van Donkelaar, A., Bai, L., Martin, R.V., Lavigne, E., Kwong, J.C., Burnett, R.T., 2020. Understanding the joint impacts of fine particulate matter concentration and composition on the incidence and mortality of cardiovascular disease: a component-adjusted approach. Environ. Sci. Technol. 54, 4388–4399. https://doi.org/10.1021/ACS.EST.9B06861.

Chen, R., Jia, B., Tian, Y., Feng, Y., 2021. Source-specific health risk assessment of $PM_{2.5}$-bound heavy metals based on high time-resolved measurement in a Chinese megacity: insights into seasonal and diurnal variations. Ecotoxicol. Environ. Saf. 216, 112167. https://doi.org/10.1016/J.ECOENV.2021.112167.

Cheung, K.L., Ntziachristos, L., Tzamkiozis, T., Schauer, J.J., Samaras, Z., Moore, K.F., Sioutas, C., 2010. Emissions of particulate trace elements, metals and organic species from gasoline, diesel, and biodiesel passenger vehicles and their relation to oxidative potential. Aerosol Sci. Technol. 44, 500–513. https://doi.org/10.1080/02786821003758294.

Cheung, R.K.Y., Qi, L., Manousakas, M.I., Puthussery, J.V., Zheng, Y., Koenig, T.K., Cui, T., Wang, T., Ge, Y., Wei, G., Kuang, Y., Sheng, M., Cheng, Z., Li, A., Li, Z., Ran, W., Xu, W., Zhang, R., Han, Y., Wang, Q., Wang, Z., Sun, Y., Cao, J., Slowik, J. G., Dällenbach, K.R., Verma, V., Gysel-Beer, M., Qiu, X., Chen, Q., Shang, J., El-Haddad, I., Prévôt, A.S.H., Modini, R.L., 2024. Major source categories of $PM_{2.5}$ oxidative potential in wintertime Beijing and surroundings based on online dithiothreitol-based field measurements. Sci. Total Environ. 928, 172345. https://doi.org/10.1016/J.SCITOTENV.2024.172345.

Chow, J.C., Lowenthal, D.H., Chen, L.-W.A., Wang, X., Watson, J.G., 2015. Mass reconstruction methods for $PM_{2.5}$: a review. Air Qual. Atmos. Health 83, 243–263. https://doi.org/10.1007/S11869-015-0338-3.

Clemente, Á., Galindo, N., Nicolás, J.F., Crespo, J., Pastor, C., Yubero, E., 2023. Local versus regional contributions to PM_{10} levels in the Western mediterranean. Aerosol Air Qual. Res. 23, 230218. https://doi.org/10.4209/AAQR.230218.

Clemente, Á., Yubero, E., Nicolás, J.F., Caballero, S., Crespo, J., Galindo, N., 2022. Changes in the concentration and composition of urban aerosols during the COVID-19 lockdown. Environ. Res. 203, 111788. https://doi.org/10.1016/J.ENVRES.2021.111788.

Creamean, J.M., Neiman, P.J., Coleman, T., Senff, C.J., Kirgis, G., Alvarez, R.J., Yamamoto, A., 2016. Colorado air quality impacted by long-range-transported aerosol: a set of case studies during the 2015 Pacific Northwest fires. Atmos. Chem. Phys. 16, 12329–12345. https://doi.org/10.5194/ACP-16-12329-2016.

Crenn, V., Sciare, J., Croteau, P.L., Verlhac, S., Fröhlich, R., Belis, C.A., Aas, W., Äijälä, M., Alastuey, A., Artiñano, B., Baisnée, D., Bonnaire, N., Bressi, M., Canagaratna, M., Canonaco, F., Carbone, C., Cavalli, F., Coz, E., Cubison, M.J., Esser-Gietl, J.K., Green, D.C., Gros, V., Heikkinen, L., Herrmann, H., Lunder, C., Minguillón, M.C., Močnik, G., O'Dowd, C.D., Ovadnevaite, J., Petit, J.E., Petralia, E., Poulain, L., Priestman, M., Riffault, V., Ripoll, A., Sarda-Estève, R., Slowik, J.G., Setyan, A., Wiedensohler, A., Baltensperger, U., Prévôt, A.S.H., Jayne, J.T., Favez, O., 2015. ACTRIS ACSM intercomparison - part 1: reproducibility of concentration and fragment results from 13 individual Quadrupole Aerosol Chemical Speciation Monitors (Q-ACSM) and consistency with co-located instruments. Atmos. Meas. Tech. 8, 5063–5087. https://doi.org/10.5194/AMT-8-5063-2015.

Crippa, M., Canonaco, F., Lanz, V.A., Äijälä, M., Allan, J.D., Carbone, S., Capes, G., Ceburnis, D., Dall'Osto, M., Day, D.A., DeCarlo, P.F., Ehn, M., Eriksson, A., Freney, E., Ruiz, L.H., Hillamo, R., Jimenez, J.L., Junninen, H., Kiendler-Scharr, A., Kortelainen, A.M., Kulmala, M., Laaksonen, A., Mensah, A.A., Mohr, C., Nemitz, E., O'Dowd, C., Ovadnevaite, J., Pandis, S.N., Petäjä, T., Poulain, L., Saarikoski, S., Sellegri, K., Swietlicki, E., Tiitta, P., Worsnop, D.R., Baltensperger, U., Prévôt, A.S.H., 2014. Organic aerosol components derived from 25 AMS data sets across Europe using a consistent ME-2 based source apportionment approach. Atmos. Chem. Phys. 14, 6159–6176. https://doi.org/10.5194/ACP-14-6159-2014.

Crippa, M., Haddad, I. El, Slowik, J.G., DeCarlo, P.F., Mohr, C., Heringa, M.F., Chirico, R., Marchand, N., Sciare, J., Baltensperger, U., Prévôt, A.S.H., 2013. Identification of marine and continental aerosol sources in Paris using high resolution aerosol mass spectrometry. J. Geophys. Res. Atmos. 118, 1950–1963. https://doi.org/10.1002/JGRD.50151.

Cuevas-Agulló, E., Barriopedro, D., García, R.D., Alonso-Pérez, S., González-Alemán, J.J., Werner, E., Suárez, D., Bustos, J.J., García-Castrillo, G., García, O., Barreto, Á., Basart, S., 2024. Sharp increase in Saharan dust intrusions over the western euro-Mediterranean in February–March 2020–2022 and associated atmospheric circulation. Atmos. Chem. Phys. 24, 4083–4104. https://doi.org/10.5194/ACP-24-4083-2024.

Dai, Q., Ding, J., Song, C., Liu, B., Bi, X., Wu, J., Zhang, Y., Feng, Y., Hopke, P.K., 2021. Changes in source contributions to particle number concentrations after the COVID-19 outbreak: insights from a dispersion normalized PMF. Sci. Total Environ. 759, 143548. https://doi.org/10.1016/J.SCITOTENV.2020.143548.

Dai, Q., Liu, B., Bi, X., Wu, J., Liang, D., Zhang, Y., Feng, Y., Hopke, P.K., 2020. Dispersion normalized PMF provides insights into the significant changes in source contributions to $PM_{2.5}$ after the COVID-19 outbreak. Environ. Sci. Technol. 54, 9917–9927. https://doi.org/10.1021/ACS.EST.0C02776.

Desouza, P., Braun, D., Parks, R.M., Schwartz, J., Dominici, F., Kioumourtzoglou, M.A., 2021. Nationwide study of short-term exposure to fine particulate matter and cardiovascular hospitalizations among medicaid enrollees. Epidemiology 32, 6–13. https://doi.org/10.1097/EDE.0000000000001265.

Di, Q., Wang, Y., Zanobetti, A., Wang, Y., Koutrakis, P., Choirat, C., Dominici, F., Schwartz, J.D., 2017. Air pollution and mortality in the medicare population. N. Engl. J. Med. 376, 2513–2522. https://doi.org/10.1056/NEJMoa1702747.

Diapouli, E., Fetfatzis, P., Panteliadis, P., Spitieri, C., Gini, M.I., Papagiannis, S., Vasilatou, V., Eleftheriadis, K., 2022. $PM_{2.5}$ source apportionment and implications for particle hygroscopicity at an urban background site in Athens, Greece. Atmosphere 13, 1685. https://doi.org/10.3390/ATMOS13101685.

Diapouli, E., Manousakas, M.I., Vratolis, S., Vasilatou, V., Pateraki, S., Bairachtari, K.A., Querol, X., Amato, F., Alastuey, A., Karanasiou, A.A., Lucarelli, F., Nava, S., Calzolai, G., Gianelle, V.L., Colombi, C., Alves, C., Custódio, D., Pio, C., Spyrou, C., Kallos, G.B., Eleftheriadis, K., 2017. AIRUSE-LIFE +: estimation of natural source contributions to urban ambient air PM_{10} and $PM_{2.5}$ concentrations in southern Europe - implications to compliance with limit values. Atmos. Chem. Phys. 17, 3673–3685. https://doi.org/10.5194/ACP-17-3673-2017.

Dimitriou, K., Grivas, G., Liakakou, E., Gerasopoulos, E., Mihalopoulos, N., 2021. Assessing the contribution of regional sources to urban air pollution by applying 3D-PSCF modeling. Atmos. Res. 248, 105187. https://doi.org/10.1016/J.ATMOSRES.2020.105187.

Dimitriou, K., Stavroulas, I., Grivas, G., Chatzidiakos, C., Kosmopoulos, G., Kazantzidis, A., Kourtidis, K., Karagioras, A., Hatzianastassiou, N., Pandis, S., Mihalopoulos, N., Gerasopoulos, E., 2023. Intra- and inter-city variability of $PM_{2.5}$ concentrations in Greece as determined with a low-cost sensor network. Atmos. Environ. 301, 119713. https://doi.org/10.1016/J.ATMOSENV.2023.119713.

Drewnick, F., Hings, S.S., Curtius, J., Eerdekens, G., Williams, J., 2006. Measurement of fine particulate and gas-phase species during the New Year's fireworks 2005 in Mainz, Germany. Atmos. Environ. 40, 4316–4327. https://doi.org/10.1016/J.ATMOSENV.2006.03.040.

Drinovec, L., Močnik, G., Zotter, P., Prévôt, A.S.H., Ruckstuhl, C., Coz, E., Rupakheti, M., Sciare, J., Müller, T., Wiedensohler, A., Wiedensohler, A., Hansen, A.D.A., 2015. The "dual-spot" aethalometer: an improved measurement of aerosol black carbon with real-time loading compensation. Atmos. Meas. Tech. 8, 1965–1979. https://doi.org/10.5194/amt-8-1965-2015.

Eiof Jonson, J., Gauss, M., Schulz, M., Jalkanen, J.P., Fagerli, H., 2020. Effects of global ship emissions on European air pollution levels. Atmos. Chem. Phys. 20, 11399–11422. https://doi.org/10.5194/ACP-20-11399-2020.

EPA, 2025. Basic Information about the Integrated Risk Information System. United States Environmental Protection Agency, 2025. https://www.epa.gov/iris/basic-information-about-integrated-risk-information-system. (Accessed 16 March 2026).

European Environment Agency, 2024. Harm to human health from air pollution – 2024. EEA Rep. No 02/2024. https://www.eea.europa.eu/en/analysis/publications/harm-to-human-health-from-air-pollution-2024.

Faisal, M., Ali, U., Kumar, A., Kumar, M., Singh, V., 2025. Unveiling $PM_{2.5}$ sources: double and tracer conjugate PMF approaches for high-resolution organic, BC, and inorganic $PM_{2.5}$ data. Atmos. Environ. 343, 121011. https://doi.org/10.1016/j.atmosenv.2024.121011.

Fajković, H., Ivanić, M., Nemet, I., Rončević, S., Kampić, Š., Vazdar, D.L., 2022. Heat–induced changes in soil properties: fires as cause for remobilization of chemical elements. J. Hydrol. Hydromechanics 70, 421–431. https://doi.org/10.2478/JOHH-2022-0024.

Fameli, K.M., Papagiannaki, K., Kotroni, V., 2021. Optimizing the knowledge on residential heating characteristics in Greece via crowd-sourcing approach. Atmosphere 12, 1178. https://doi.org/10.3390/ATMOS12091178.

Fameli, K.M., Assimakopoulos, V.D., 2015. Development of a road transport emission inventory for Greece and the greater Athens area: effects of important parameters. Sci. Total Environ. 505, 770–786. https://doi.org/10.1016/J.SCITOTENV.2014.10.015.

Fang, T., Guo, H., Verma, V., Peltier, R.E., Weber, R.J., 2015. $PM_{2.5}$ water-soluble elements in the southeastern United States: automated analytical method development, spatiotemporal distributions, source apportionment, and implications for health studies. Atmos. Chem. Phys. 15, 11667–11682. https://doi.org/10.5194/ACP-15-11667-2015.

Fisher, J.A., Puett, R.C., Laden, F., Wellenius, G.A., Sapkota, A., Liao, D., Yanosky, J.D., Carter-Pokras, O., He, X., Hart, J.E., 2019. Case-crossover analysis of short-term particulate matter exposures and stroke in the health professionals follow-up study. Environ. Int. 124, 153–160. https://doi.org/10.1016/J.ENVINT.2018.12.044.

Florou, K., Papanastasiou, D.K., Pikridas, M., Kaltsonoudis, C., Louvaris, E., Gkatzelis, G. I., Patoulias, D., Mihalopoulos, N., Pandis, S.N., 2017. The contribution of wood burning and other pollution sources to wintertime organic aerosol levels in two Greek cities. Atmos. Chem. Phys. 17, 3145–3163. https://doi.org/10.5194/ACP-17-3145-2017.

Formenti, P., Elbert, W., Maenhaut, W., Haywood, J., Andreae, M.O., 2003. Chemical composition of mineral dust aerosol during the Saharan Dust Experiment (SHADE) airborne campaign in the Cape Verde region, 2000. J. Geophys. Res. Atmos. 108, 8576. https://doi.org/10.1029/2002JD002648.

Fourtziou, L., Liakakou, E., Stavroulas, I., Theodosi, C., Zarmpas, P., Psiloglou, B., Sciare, J., Maggos, T., Bairachtari, K., Bougiatioti, A., Bonnaire, N., Mihalopoulos, N., 2017. Multi-tracer approach to characterize domestic wood burning in Athens (Greece) during wintertime. Atmos. Environ. 148, 89–101. https://doi.org/10.1016/j.atmosenv.2016.10.011.

Fragkou, E., Tsegas, G., Alyuz, U., Hänninen, R., Moldanova, J., Jutterström, S., Majamäki, E., Jalkanen, J.P., Sokhi, R.S., Kukkonen, J., Sofiev, M., Ntziachristos, L., 2025. Assessing the efficiency of different mitigation strategies to reduce shipping related air pollution levels and exposure in the Mediterranean coastal region – an ensemble modelling approach. Atmos. Environ. 360, 121347. https://doi.org/10.1016/J.ATMOSENV.2025.121347.

Freney, E., Zhang, Y., Croteau, P., Amodeo, T., Williams, L., Truong, F., Petit, J.-E., Sciare, J., Sarda-Esteve, R., Bonnaire, N., Arumae, T., Aurela, M., Bougiatioti, A., Mihalopoulos, N., Coz, E., Artinano, B., Crenn, V., Elste, T., Heikkinen, L., Poulain, L., Wiedensohler, A., Herrmann, H., Priestman, M., Alastuey, A., Stavroulas, I., Tobler, A., Vasilescu, J., Zanca, N., Canagaratna, M., Carbone, C., Flentje, H., Green, D., Maasikmets, M., Marmureanu, L., Minguillon, M.C., Prevot, A. S.H., Gros, V., Jayne, J., Favez, O., 2019. The second ACTRIS inter-comparison (2016) for Aerosol Chemical Speciation Monitors (ACSM): calibration protocols and instrument performance evaluations. Aerosol Sci. Technol. 53, 830–842. https://doi.org/10.1080/02786826.2019.1608901.

Furger, M., Minguillón, M.C., Yadav, V., Slowik, J.G., Hüglin, C., Fröhlich, R., Petterson, K., Baltensperger, U., Prévôt, A.S.H., 2017. Elemental composition of ambient aerosols measured with high temporal resolution using an online XRF spectrometer. Atmos. Meas. Tech. 10, 2061–2076. https://doi.org/10.5194/AMT-10-2061-2017.

Fussell, J.C., Franklin, M., Green, D.C., Gustafsson, M., Harrison, R.M., Hicks, W., Kelly, F.J., Kishta, F., Miller, M.R., Mudway, I.S., Oroumiyeh, F., Selley, L., Wang, M., Zhu, Y., 2022. A review of road traffic-derived non-exhaust particles: emissions, physicochemical characteristics, health risks, and mitigation measures. Environ. Sci. Technol. 56, 6813–6835. https://doi.org/10.1021/ACS.EST.2C01072.

Galindo, N., Yubero, E., Nicolás, J.F., Varea, M., Crespo, J., 2018. Characterization of metals in PM_1 and PM_{10} and health risk evaluation at an urban site in the western Mediterranean. Chemosphere 201, 243–250. https://doi.org/10.1016/J.CHEMOSPHERE.2018.02.162.

Gerasopoulos, E., Amiridis, V., Kazadzis, S., Kokkalis, P., Eleftheratos, K., Andreae, M.O., Andreae, T.W., El-Askary, H., Zerefos, C.S., 2011. Three-year ground based measurements of aerosol optical depth over the Eastern Mediterranean: the urban environment of Athens. Atmos. Chem. Phys. 11, 2145–2159. https://doi.org/10.5194/acp-11-2145-2011.

Giannaros, T.M., Lagouvardos, K., Kotroni, V., 2020. Performance evaluation of an operational rapid response fire spread forecasting system in the Southeast Mediterranean (Greece). Atmosphere 11, 1264. https://doi.org/10.3390/ATMOS11111264.

Giannaros, T.M., Papavasileiou, G., Lagouvardos, K., Kotroni, V., Dafis, S., Karagiannidis, A., Dragozi, E., 2022. Meteorological analysis of the 2021 extreme wildfires in Greece: lessons learned and implications for early warning of the potential for pyroconvection. Atmosphere 13, 475. https://doi.org/10.3390/ATMOS13030475.

Gini, M., Manousakas, M., Karydas, A.G., Eleftheriadis, K., 2022. Mass size distributions, composition and dose estimates of particulate matter in Saharan dust outbreaks. Environ. Pollut. 298, 118768. https://doi.org/10.1016/J.ENVPOL.2021.118768.

Goldberger, L.A., Jahl, L.G., Thornton, J.A., Sullivan, R.C., 2019. N_2O_5 reactive uptake kinetics and chlorine activation on authentic biomass-burning aerosol. Environ. Sci. Process. Impacts 21, 1684–1698. https://doi.org/10.1039/C9EM00330D.

Grigoratos, T., Martini, G., 2014. Brake wear particle emissions: a review. Environ. Sci. Pollut. Res. 22, 2491–2504. https://doi.org/10.1007/S11356-014-3696-8.
Grivas, G., Athanasopoulou, E., Kakouri, A., Bailey, J., Liakakou, E., Stavroulas, I., Kalkavouras, P., Bougiatioti, A., Kaskaoutis, D.G., Ramonet, M., Mihalopoulos, N., Gerasopoulos, E., 2020. Integrating in situ measurements and city scale modelling to assess the COVID–19 lockdown effects on emissions and air quality in Athens, Greece. Atmosphere 11, 1174. https://doi.org/10.3390/ATMOS11111174.
Grivas, G., Cheristanidis, S., Chaloulakou, A., 2012. Elemental and organic carbon in the urban environment of Athens. Seasonal and diurnal variations and estimates of secondary organic carbon. Sci. Total Environ. 414, 535–545. https://doi.org/10.1016/J.SCITOTENV.2011.10.058.
Grivas, G., Cheristanidis, S., Chaloulakou, A., Koutrakis, P., Mihalopoulos, N., 2018. Elemental composition and source apportionment of fine and coarse particles at traffic and urban background locations in Athens, Greece. Aerosol Air Qual. Res. 18, 1642–1659. https://doi.org/10.4209/AAQR.2017.12.0567.
Hamad, S., Green, D., Heo, J., 2016. Evaluation of health risk associated with fireworks activity at Central London. Air Qual. Atmos. Health 9, 735–741. https://doi.org/10.1007/s11869-015-0384-x.
Harrison, R.M., Allan, J., Carruthers, D., Heal, M.R., Lewis, A.C., Marner, B., Murrells, T., Williams, A., 2021. Non-exhaust vehicle emissions of particulate matter and VOC from road traffic: a review. Atmos. Environ. 262, 118592. https://doi.org/10.1016/J.ATMOSENV.2021.118592.
Hasheminassab, S., Sowlat, M.H., Pakbin, P., Katzenstein, A., Low, J., Polidori, A., 2020. High time-resolution and time-integrated measurements of particulate metals and elements in an environmental justice community within the Los Angeles Basin: Spatio-temporal trends and source apportionment. Atmos. Environ. X (7), 100089. https://doi.org/10.1016/j.aeaoa.2020.100089.
Hemmingsen, J.G., Rissler, J., Lykkesfeldt, J., Sallsten, G., Kristiansen, J., P, P.M., Loft, S., 2015. Controlled exposure to particulate matter from urban street air is associated with decreased vasodilation and heart rate variability in overweight and older adults. Part. Fibre Toxicol. 12, 1–10. https://doi.org/10.1186/S12989-015-0081-9.
Hicks, W., Beevers, S., Tremper, A.H., Stewart, G., Priestman, M., Kelly, F.J., Lanoisellé, M., Lowry, D., Green, D.C., 2021. Quantification of non-exhaust particulate matter traffic emissions and the impact of COVID-19 lockdown at London marylebone road. Atmosphere 12, 190. https://doi.org/10.3390/ATMOS12020190.
Hong, Y., Xu, X., Liao, D., Zheng, R., Ji, X., Chen, Y., Xu, L., Li, M., Wang, H., Xiao, H., Choi, S.D., Chen, J., 2021. Source apportionment of $PM_{2.5}$ and sulfate formation during the COVID-19 lockdown in a coastal city of southeast China. Environ. Pollut. 286, 117577. https://doi.org/10.1016/J.ENVPOL.2021.117577.
Hu, X., Zhang, Y., Ding, Z., Wang, T., Lian, H., Sun, Y., Wu, J., 2012. Bioaccessibility and health risk of arsenic and heavy metals (Cd, Co, Cr, Cu, Ni, Pb, Zn and Mn) in TSP and $PM_{2.5}$ in Nanjing, China. Atmos. Environ. Times 57, 146–152. https://doi.org/10.1016/J.ATMOSENV.2012.04.056.
Huang, S., Taddei, P., Lawrence, J., Martins, M.A.G., Li, J., Koutrakis, P., 2021. Trace element mass fractions in road dust as a function of distance from road. J. Air Waste Manag. Assoc. 71, 137–146. https://doi.org/10.1080/10962247.2020.1834011.
Im, U., Markakis, K., Koçak, M., Gerasopoulos, E., Daskalakis, N., Mihalopoulos, N., Poupkou, A., Kindap, T., Unal, A., Kanakidou, M., 2012. Summertime aerosol chemical composition in the Eastern Mediterranean and its sensitivity to temperature. Atmos. Environ. 50, 164–173. https://doi.org/10.1016/J.ATMOSENV.2011.12.044.
Ito, A., Miyakawa, T., 2023. Aerosol Iron from metal production as a secondary source of bioaccessible iron. Environ. Sci. Technol. 57, 4091–4100. https://doi.org/10.1021/ACS.EST.2C06472.
Jang, E., Choi, S., Yoo, E., Hyun, S., An, J., 2023. Impact of shipping emissions regulation on urban aerosol composition changes revealed by receptor and numerical modelling. npj Clim. Atmos. Sci. 6, 52. https://doi.org/10.1038/s41612-023-00364-9, 2023.
Janta, R., Tala, W., Kaeway, K., Sumrajgij, U., Muenrew, J., Yabueng, N., Chantara, S., 2025. Diurnal health risk assessment of potentially toxic elements in $PM_{2.5}$ for children and adults in upper Southeast Asia during the smoke haze period. J. Hazard. Mater. Adv. 19, 100807. https://doi.org/10.1016/J.HAZADV.2025.100807.
Jeong, C.H., Yousif, M., Evans, G.J., 2022. Impact of the COVID-19 lockdown on the chemical composition and sources of urban $PM_{2.5}$. Environ. Pollut. 292, 118417. https://doi.org/10.1016/J.ENVPOL.2021.118417.
Jorga, S.D., Florou, K., Kaltsonoudis, C., Kodros, J.K., Vasilakopoulou, C., Cirtog, M., Fouqueau, A., Picquet-Varrault, B., Nenes, A., Pandis, S.N., 2021. Nighttime chemistry of biomass burning emissions in urban areas: a dual mobile chamber study. Atmos. Chem. Phys. 21, 15337–15349. https://doi.org/10.5194/acp-21-15337-2021.
Kalivitis, N., Gerasopoulos, E., Vrekoussis, M., Kouvarakis, G., Kubilay, N., Hatzianastassiou, N., Vardavas, I., Mihalopoulos, N., 2007. Dust transport over the eastern mediterranean derived from total ozone mapping spectrometer, aerosol robotic network, and surface measurements. J. Geophys. Res. Atmos. 112, 3202. https://doi.org/10.1029/2006JD007510.
Kalkavouras, P., Bougiatioti, A., Grivas, G., Stavroulas, I., Kalivitis, N., Liakakou, E., Gerasopoulos, E., Pilinis, C., Mihalopoulos, N., 2020. On the regional aspects of new particle formation in the Eastern Mediterranean: a comparative study between a background and an urban site based on long term observations. Atmos. Res. 239, 104911. https://doi.org/10.1016/J.ATMOSRES.2020.104911.
Kalkavouras, P., Grivas, G., Stavroulas, I., Petrinoli, K., Bougiatioti, A., Liakakou, E., Gerasopoulos, E., Mihalopoulos, N., 2024. Source apportionment of fine and ultrafine particle number concentrations in a major city of the Eastern Mediterranean. Sci. Total Environ. 915, 170042. https://doi.org/10.1016/J.SCITOTENV.2024.170042.
Kalkschmied, K., Stricker, P., 2026. Critical infrastructure, critical trade-offs: the growth effects of Chinese investments in European ports. Transp. Res. Part A Policy Pract. 203, 104704. https://doi.org/10.1016/J.TRA.2025.104704.
Kaskaoutis, D.G., Petrinoli, K., Grivas, G., Kalkavouras, P., Tsagkaraki, M., Tavernaraki, K., Papoutsidaki, K., Stavroulas, I., Paraskevopoulou, D., Bougiatioti, A., Liakakou, E., Rashki, A., Sotiropoulou, R.E.P., Tagaris, E., Gerasopoulos, E., Mihalopoulos, N., 2024. Impact of peri-urban forest fires on air quality and aerosol optical and chemical properties: the case of the August 2021 wildfires in Athens, Greece. Sci. Total Environ. 907, 168028. https://doi.org/10.1016/J.SCITOTENV.2023.168028.
Kassomenos, P., Flocas, H.A., Lykoudis, S., Petrakis, M., 1998. Analysis of mesoscale patterns in relation to synoptic conditions over an urban Mediterranean basin. Theor. Appl. Climatol. 59, 215–229. https://doi.org/10.1007/S007040050025, 1998.
Kelesidis, G.A., Moularas, C., Parhizkar, H., Calderon, L., Tsiodra, I., Mihalopoulos, N., Kavouras, I., Korras-Carraca, M.B., Hatzianastassiou, N., Georgopoulos, P.G., Cedeño Laurent, J.G., Demokritou, P., 2025. Radiative cooling in New York/New Jersey metropolitan areas by wildfire particulate matter emitted from the Canadian wildfires of 2023. Commun. Earth Environ. 6, 304. https://doi.org/10.1038/s43247-025-02214-3, 2025.
Kirchstetter, T.W., Thatcher, T.L., 2012. Contribution of organic carbon to wood smoke particulate matter absorption of solar radiation. Atmos. Chem. Phys. 12, 6067–6072. https://doi.org/10.5194/ACP-12-6067-2012.
Koch, E.C., 2015. Spectral investigation and color properties of Copper(I) Halides CuX (X=F, Cl, Br, I) in pyrotechnic combustion flames. Propellants, Explos. Pyrotech. 40, 799–802. https://doi.org/10.1002/PREP.201500231.
Kokkalis, P., Soupiona, O., Papanikolaou, C.A., Foskinis, R., Mylonaki, M., Solomos, S., Vratolis, S., Vasilatou, V., Kralli, E., Anagnou, D., Papayannis, A., 2021. Radiative effect and mixing processes of a long-lasting dust event over Athens, Greece, during the COVID-19 period. Atmosphere 12, 318. https://doi.org/10.3390/ATMOS12030318.
Krall, J.R., Chang, H.H., Waller, L.A., Mulholland, J.A., Winquist, A., Talbott, E.O., Rager, J.R., Tolbert, P.E., Sarnat, S.E., 2018. A multicity study of air pollution and cardiorespiratory emergency department visits: comparing approaches for combining estimates across cities. Environ. Int. 120, 312–320. https://doi.org/10.1016/J.ENVINT.2018.07.033.
Kukkonen, J., López-Aparicio, S., Segersson, D., Geels, C., Kangas, L., Kauhaniemi, M., Maragkidou, A., Jensen, A., Assmuth, T., Karppinen, A., Sofiev, M., Hellén, H., Riikonen, K., Nikmo, J., Kousa, A., Niemi, J.V., Karvosenoja, N., Sousa Santos, G., Sundvor, I., Im, U., Christensen, J.H., Nielsen, O.K., Plejdrup, M.S., Klenø Nøjgaard, J., Omstedt, G., Andersson, C., Forsberg, B., Brandt, J., 2020. The influence of residential wood combustion on the concentrations of $PM_{2.5}$ in four Nordic cities. Atmos. Chem. Phys. 20, 4333–4365. https://doi.org/10.5194/ACP-20-4333-2020.
Lakra, A., Kumar, A., Sethi, D., Bhowmik, H.S., Jain, V., Tripathi, S.N., 2026. High-resolution source apportionment and health risks of $PM_{2.5}$-bound trace elements across a major Indian city: seasonal and diurnal insights from a multi-site campaign using a mobile laboratory platform. Atmos. Environ. 365, 121675. https://doi.org/10.1016/J.ATMOSENV.2025.121675.
Le Berre, L., Temime-Roussel, B., Lanzafame, G.M., D'Anna, B., Marchand, N., Sauvage, S., Dufresne, M., Tinel, L., Leonardis, T., de Brito, J.F., Armengaud, A., Gille, G., Lanzi, L., Bourjot, R., Wortham, H., 2025. Measurement report: in-depth characterization of ship emissions during operations in a Mediterranean port. Atmos. Chem. Phys. 25, 6575–6605. https://doi.org/10.5194/acp-25-6575-2025.
Li, Y., Kleimann, M., Schmerer, H.J., 2021. Estimating causal effects of BRI infrastructure projects based on the synthetic control method. Asia Eur. J. 19, 103–129. https://doi.org/10.1007/S10308-021-00621-7.
Li, Y., Yao, L., Yang, J., Wu, J., Tang, X., Liang, S., Zhang, Y., Feng, Y., 2024. Characterizing the emission trends and pollution evolution patterns during the transition period following COVID-19 at an industrial megacity of central China. Ecotoxicol. Environ. Saf. 278, 116354. https://doi.org/10.1016/J.ECOENV.2024.116354.
Li, Z., Hopke, P.K., Husain, L., Qureshi, S., Dutkiewicz, V.A., Schwab, J.J., Drewnick, F., Demerjian, K.L., 2004. Sources of fine particle composition in New York city. Atmos. Environ. 38, 6521–6529. https://doi.org/10.1016/J.ATMOSENV.2004.08.040.
Liakakou, E., Stavroulas, I., Kaskaoutis, D.G., Grivas, G., Paraskevopoulou, D., Dumka, U. C., Tsagkaraki, M., Bougiatioti, A., Oikonomou, K., Sciare, J., Gerasopoulos, E., Mihalopoulos, N., 2020. Long-term variability, source apportionment and spectral properties of black carbon at an urban background site in Athens, Greece. Atmos. Environ. 222. https://doi.org/10.1016/j.atmosenv.2019.117137.
Liu, C., Chen, R., Sera, F., Vicedo-Cabrera, A.M., Guo, Y., Tong, S., Coelho, M.S.Z.S., Saldiva, P.H.N., Lavigne, E., Matus, P., Valdes Ortega, N., Osorio Garcia, S., Pascal, M., Stafoggia, M., Scortichini, M., Hashizume, M., Honda, Y., Hurtado-Díaz, M., Cruz, J., Nunes, B., Teixeira, J.P., Kim, H., Tobias, A., Íñiguez, C., Forsberg, B., Åström, C., Ragettli, M.S., Guo, Y.-L., Chen, B.-Y., Bell, M.L., Wright, C. Y., Scovronick, N., Garland, R.M., Milojevic, A., Kyselý, J., Urban, A., Orru, H., Indermitte, E., Jaakkola, J.J.K., Ryti, N.R.I., Katsouyanni, K., Analitis, A., Zanobetti, A., Schwartz, J., Chen, J., Wu, T., Cohen, A., Gasparrini, A., Kan, H., 2019a. Ambient particulate air pollution and daily mortality in 652 cities. N. Engl. J. Med. 381, 705–715. https://doi.org/10.1056/NEJMOA1817364.
Liu, H., Song, D., Zhang, X., Huang, F., Hu, X., 2020. A study on characteristics of heavy metal elements in atmospheric $PM_{2.5}$ during winter in Chengdu. IOP Conf. Ser. Earth Environ. Sci. 514. https://doi.org/10.1088/1755-1315/514/3/032046.
Liu, X., Zheng, M., Liu, Y., Jin, Y., Liu, J., Zhang, B., Yang, X., Wu, Y., Zhang, T., Xiang, Y., Liu, B., Yan, C., 2022. Intercomparison of equivalent black carbon (eBC) and elemental carbon (EC) concentrations with three-year continuous measurement

in Beijing, China. Environ. Res. 209, 112791. https://doi.org/10.1016/J.ENVRES.2022.112791.
Liu, Y., Yan, C., Zheng, M., 2018. Source apportionment of black carbon during winter in Beijing. Sci. Total Environ. 618, 531–541. https://doi.org/10.1016/j.scitotenv.2017.11.053.
Liu, Y., Zheng, M., Yu, M., Cai, X., Du, H., Li, J., Zhou, T., Yan, C., Wang, X., Shi, Z., Harrison, R.M., Zhang, Q., He, K., 2019b. High-time-resolution source apportionment of $PM_{2.5}$ in Beijing with multiple models. Atmos. Chem. Phys. 19, 6595–6609. https://doi.org/10.5194/ACP-19-6595-2019.
Lopez, B., Wang, X., Chen, L.W.A., Ma, T., Mendez-Jimenez, D., Cobb, L.C., Frederickson, C., Fang, T., Hwang, B., Shiraiwa, M., Park, M., Park, K., Yao, Q., Yoon, S., Jung, H., 2023. Metal contents and size distributions of brake and tire wear particles dispersed in the near-road environment. Sci. Total Environ. 883, 163561. https://doi.org/10.1016/J.SCITOTENV.2023.163561.
Mach, T., Rogula-Kozłowska, W., Bralewska, K., Majewski, G., Rogula-Kopiec, P., Rybak, J., 2021. Impact of municipal, road traffic, and natural sources on PM_{10}: the hourly variability at a rural site in Poland. Energies 14, 2654. https://doi.org/10.3390/EN14092654.
Mach, T., Rybak, J., Bihałowicz, J., Rogula-Kozłowska, W., 2022. Quasi real-time X-Ray Fluorescence spectrometer in source apportionment of particulate matter in a typical suburban area. J. Ecol. Eng. 23, 89–97. https://doi.org/10.12911/22998993/152282.
Makkonen, U., Virkkula, A., Mäntykenttä, J., Hakola, H., Keronen, P., Vakkari, V., Aalto, P.P., 2012. Semi-continuous gas and inorganic aerosol measurements at a Finnish urban site: comparisons with filters, nitrogen in aerosol and gas phases, and aerosol acidity. Atmos. Chem. Phys. 12, 5617–5631. https://doi.org/10.5194/ACP-12-5617-2012.
Manousakas, M., Diapouli, E., Belis, C., Vasilatou, V., Gini, M., Lucarelli, F., Querol, X., Eleftheriadis, K., 2021. Quantitative assessment of the variability in chemical profiles from source apportionment analysis of PM_{10} and $PM_{2.5}$ at different sites within a large metropolitan area. Environ. Res. 192, 110257. https://doi.org/10.1016/J.ENVRES.2020.110257.
Manousakas, M., Furger, M., Daellenbach, K.R., Canonaco, F., Chen, G., Tobler, A., Rai, P., Qi, L., Tremper, A.H., Green, D., Hueglin, C., Slowik, J.G., El Haddad, I., Prevot, A.S.H., 2022. Source identification of the elemental fraction of particulate matter using size segregated, highly time-resolved data and an optimized source apportionment approach. Atmos. Environ. X 14, 100165. https://doi.org/10.1016/J.AEAOA.2022.100165.
Manousakas, M.I., Zografou, O., Canonaco, F., Diapouli, E., Papagiannis, S., Gini, M., Vasilatou, V., Tobler, A., Vratolis, S., Slowik, J.G., Daellenbach, K.R., Prevot, A.S.H., Eleftheriadis, K., 2025. Implementation of real-Time source apportionment approaches using the ACSM-Xact-Aethalometer (AXA) setup with SoFi RT: the Athens case study. Atmos. Meas. Tech. 18, 3983–4002. https://doi.org/10.5194/AMT-18-3983-2025.
Marconi, M., Sferlazzo, D.M., Becagli, S., Bommarito, C., Calzolai, G., Chiari, M., Di Sarra, A., Ghedini, C., Gómez-Amo, J.L., Lucarelli, F., Meloni, D., Monteleone, F., Nava, S., Pace, G., Piacentino, S., Rugi, F., Severi, M., Traversi, R., Udisti, R., 2014. Saharan dust aerosol over the central Mediterranean Sea: PM_{10} chemical composition and concentration versus optical columnar measurements. Atmos. Chem. Phys. 14, 2039–2054. https://doi.org/10.5194/ACP-14-2039-2014.
Menut, L., Siour, G., Bessagnet, B., Cholakian, A., Pennel, R., Mailler, S., 2022. Impact of wildfires on mineral dust emissions in Europe. J. Geophys. Res. Atmos. 127. https://doi.org/10.1029/2022JD037395 e2022JD037395.
Miyakawa, T., Ito, A., Zhu, C., Shimizu, A., Matsumoto, E., Mizuno, Y., Kanaya, Y., 2023. Trace elements in $PM_{2.5}$ aerosols in East Asian outflow in the spring of 2018: emission, transport, and source apportionment. Atmos. Chem. Phys. 23, 14609–14626. https://doi.org/10.5194/ACP-23-14609-2023.
Müller, K., Unice, K., Panko, J., Wagner, S., 2025. Tire emissions during the use phase of tires – current and future trends. Environ. Sci. Adv. 4, 1344–1363. https://doi.org/10.1039/D4VA00407H.
Möring-Martínez, G., Senzeybek, M., Hasselwander, S., Schmid, S., 2025. Quantifying the impact of fleet turnover on electric vehicle uptake in Europe. Transp. Res., Part D Transp. Environ. 147, 104945. https://doi.org/10.1016/J.TRD.2025.104945.
Ng, N.L., Canagaratna, M.R., Jimenez, J.L., Zhang, Q., Ulbrich, I.M., Worsnop, D.R., 2010. Real-time methods for estimating organic component mass concentrations from aerosol mass spectrometer data. Environ. Sci. Technol. 45, 910–916. https://doi.org/10.1021/ES102951K.
Ng, N.L., Herndon, S.C., Trimborn, A., Canagaratna, M.R., Croteau, P.L., Onasch, T.B., Sueper, D., Worsnop, D.R., Zhang, Q., Sun, Y.L., Jayne, J.T., 2011. An Aerosol Chemical Speciation Monitor (ACSM) for routine monitoring of the composition and mass concentrations of ambient aerosol. Aerosol Sci. Technol. 45, 780–794. https://doi.org/10.1080/02786826.2011.560211.
NIST, 2011. Certificate of Analysis — Standard Reference Material 2783: Air Particulate on Filter Media. Gaithersburg, MD.
Orach, J., Rider, C.F., Carlsten, C., 2021. Concentration-dependent health effects of air pollution in controlled human exposures. Environ. Int. 150, 106424. https://doi.org/10.1016/J.ENVINT.2021.106424.
Orsini, D.A., Ma, Y., Sullivan, A., Sierau, B., Baumann, K., Weber, R.J., 2003. Refinements to the particle-into-liquid sampler (PILS) for ground and airborne measurements of water soluble aerosol composition. Atmos. Environ. 37, 1243–1259. https://doi.org/10.1016/S1352-2310(02)01015-4.
Ostro, B., Malig, B., Hasheminassab, S., Berger, K., Chang, E., Sioutas, C., 2016. Associations of source-specific fine particulate matter with emergency department visits in California. Am. J. Epidemiol. 184, 450–459. https://doi.org/10.1093/AJE/KWV343.
Paatero, P., Eberly, S., Brown, S.G., Norris, G.A., 2014. Methods for estimating uncertainty in factor analytic solutions. Atmos. Meas. Tech. 7, 781–797. https://doi.org/10.5194/AMT-7-781-2014.
Pandis, S.N., Skyllakou, K., Florou, K., Kostenidou, E., Kaltsonoudis, C., Hasa, E., Presto, A.A., 2016. Urban particulate matter pollution: a tale of five cities. Faraday Discuss. 189, 277–290. https://doi.org/10.1039/C5FD00212E.
Pandolfi, M., Alastuey, A., Pérez, N., Reche, C., Castro, I., Shatalov, V., Querol, X., 2016. Trends analysis of PM source contributions and chemical tracers in NE Spain during 2004-2014: a multi-exponential approach. Atmos. Chem. Phys. 16, 11787–11805. https://doi.org/10.5194/acp-16-11787-2016.
Paraskevopoulou, D., Bougiatioti, A., Stavroulas, I., Fang, T., Lianou, M., Liakakou, E., Gerasopoulos, E., Weber, R., Nenes, A., Mihalopoulos, N., 2019. Yearlong variability of oxidative potential of particulate matter in an urban Mediterranean environment. Atmos. Environ. 206, 183–196. https://doi.org/10.1016/j.atmosenv.2019.02.027.
Paraskevopoulou, D., Kaskaoutis, D.G., Grivas, G., Bikkina, S., Tsagkaraki, M., Vrettou, I. M., Tavernaraki, K., Papoutsidaki, K., Stavroulas, I., Liakakou, E., Bougiatioti, A., Oikonomou, K., Gerasopoulos, E., Mihalopoulos, N., 2023. Brown carbon absorption and radiative effects under intense residential wood burning conditions in Southeastern Europe: new insights into the abundance and absorptivity of methanol-soluble organic aerosols. Sci. Total Environ. 860, 160434. https://doi.org/10.1016/J.SCITOTENV.2022.160434.
Pereira, P., Úbeda, X., Martin, D.A., 2012. Fire severity effects on ash chemical composition and water-extractable elements. Geoderma 191, 105–114. https://doi.org/10.1016/J.GEODERMA.2012.02.005.
Perron, M.M.G., Meyerink, S., Corkill, M., Strzelec, M., Proemse, B.C., Gault-Ringold, M., Sanz Rodriguez, E., Chase, Z., Bowie, A.R., 2022. Trace elements and nutrients in wildfire plumes to the southeast of Australia. Atmos. Res. 270, 106084. https://doi.org/10.1016/J.ATMOSRES.2022.106084.
Petit, J.E., Favez, O., Albinet, A., Canonaco, F., 2017. A user-friendly tool for comprehensive evaluation of the geographical origins of atmospheric pollution: wind and trajectory analyses. Environ. Model. Software 88, 183–187. https://doi.org/10.1016/J.ENVSOFT.2016.11.022.
Petrinoli, K., Kaskaoutis, D.G., Bougiatioti, A., Liakakou, E., Grivas, G., Kalkavouras, P., Mihalopoulos, N., 2025. Year-long variability of the mixing layer height at an urban Mediterranean location and association with air pollution levels. Atmos. Pollut. Res. 16, 102612. https://doi.org/10.1016/J.APR.2025.102612.
Pey, J., Pérez, N., Cortés, J., Alastuey, A., Querol, X., 2013. Chemical fingerprint and impact of shipping emissions over a western Mediterranean metropolis: primary and aged contributions. Sci. Total Environ. 463–464, 497–507. https://doi.org/10.1016/J.SCITOTENV.2013.06.061.
Pio, C., Cerqueira, M., Harrison, R.M., Nunes, T., Mirante, F., Alves, C., Oliveira, C., Sanchez de la Campa, A., Artíñano, B., Matos, M., 2011. OC/EC ratio observations in Europe: Re-thinking the approach for apportionment between primary and secondary organic carbon. Atmos. Environ. 45, 6121–6132. https://doi.org/10.1016/J.ATMOSENV.2011.08.045.
Poupkou, A., Liora, N., Kontos, S., Grivas, G., Fameli, K.-M., Tsiaousidis, D., Solomos, S., Kapsomenakis, I., Assimakopoulos, V., Progiou, A., Kalabokas, P., Mihalopoulos, N., Kotrikla, A.M., Melas, D., Zerefos, C., 2026. Assessing the impact of ship emissions on the atmospheric chemical composition in the Eastern Mediterranean and the Piraeus port (Greece). Sci. Rep. 161, 3805. https://doi.org/10.1038/s41598-025-33968-7.
Rai, P., Furger, M., Slowik, J.G., Canonaco, F., Fröhlich, R., Hüglin, C., Minguillón, M.C., Petterson, K., Baltensperger, U., Prévôt, A.S.H., 2020. Source apportionment of highly time-resolved elements during a firework episode from a rural freeway site in Switzerland. Atmos. Chem. Phys. 20, 1657–1674. https://doi.org/10.5194/acp-20-1657-2020.
Reff, A., Eberly, S.I., Bhave, P.V., 2007. Receptor modeling of ambient particulate matter data using positive matrix factorization: review of existing methods. J. Air Waste Manag. Assoc. 57, 146–154. https://doi.org/10.1080/10473289.2007.10465319.
Ryder, O.S., DeWinter, J.L., Brown, S.G., Hoffman, K., Frey, B., Mirzakhalili, A., 2020. Assessment of particulate toxic metals at an environmental justice community. Atmos. Environ. X 6, 100070. https://doi.org/10.1016/j.aeaoa.2020.100070.
Saliba, M., Azzopardi, F., Muscat, R., Grima, M., Smyth, A., Jalkanen, J.P., Johansson, L., Deidun, A., Gauci, A., Galdies, C., Caruana, T., Ellul, R., 2021. Trends in vessel atmospheric emissions in the central Mediterranean over the last 10 years and during the COVID-19 outbreak. J. Mar. Sci. Eng. 9, 762. https://doi.org/10.3390/JMSE9070762.
Sandradewi, J., Prévôt, A.S.H., Szidat, S., Perron, N., Alfarra, M.R., Lanz, V.A., Weingartner, E., Baltensperger, U., 2008. Using aerosol light absorption measurements for the quantitative determination of wood burning and traffic emission contributions to particulate matter. Environ. Sci. Technol. 42, 3316–3323. https://doi.org/10.1021/ES702253M.
Saraga, D., Maggos, T., Degrendele, C., Klánová, J., Horvat, M., et al., 2021. Multi-city comparative PM2.5 source apportionment for fifteen sites in Europe: The ICARUS project. Sci. Total Environ. 751, 141855. https://doi.org/10.1016/j.scitotenv.2020.141855, 141855.
Savadkoohi, M., Gherras, M., Favez, O., Petit, J.E., Rovira, J., Chen, G.I., Via, M., Platt, S., Aurela, M., Chazeau, B., de Brito, J.F., Riffault, V., Eleftheriadis, K., Flentje, H., Gysel-Beer, M., Hueglin, C., Rigler, M., Gregorič, A., Ivančič, M., Keernik, H., Maasikmets, M., Liakakou, E., Stavroulas, I., Luoma, K., Marchand, N., Mihalopoulos, N., Petäjä, T., Prevot, A.S.H., Daellenbach, K.R., Vodička, P., Timonen, H., Tobler, A., Vasilescu, J., Dandocsi, A., Mbengue, S., Vratolis, S., Zografou, O., Chauvigné, A., Hopke, P.K., Querol, X., Alastuey, A., Pandolfi, M., 2025. Addressing the advantages and limitations of using Aethalometer data to determine the optimal absorption Ångström exponents (AAEs) values for eBC source

apportionment. Atmos. Environ. 349, 121121. https://doi.org/10.1016/J.ATMOSENV.2025.121121.

Savadkoohi, M., Pandolfi, M., Reche, C., Niemi, J.V., Mooibroek, D., Titos, G., Green, D. C., Tremper, A.H., Hueglin, C., Liakakou, E., Mihalopoulos, N., Stavroulas, I., Artiñano, B., Coz, E., Alados-Arboledas, L., Beddows, D., Riffault, V., De Brito, J.F., Bastian, S., Baudic, A., Colombi, C., Costabile, F., Chazeau, B., Marchand, N., Gómez-Amo, J.L., Estellés, V., Matos, V., van der Gaag, E., Gille, G., Luoma, K., Manninen, H.E., Norman, M., Silvergren, S., Petit, J.E., Putaud, J.P., Rattigan, O.V., Timonen, H., Tuch, T., Merkel, M., Weinhold, K., Vratolis, S., Vasilescu, J., Favez, O., Harrison, R.M., Laj, P., Wiedensohler, A., Hopke, P.K., Petäjä, T., Alastuey, A., Querol, X., 2023. The variability of mass concentrations and source apportionment analysis of equivalent black carbon across urban Europe. Environ. Int. 178, 108081. https://doi.org/10.1016/J.ENVINT.2023.108081.

Schulte-Fischedick, M., Shan, Y., Hubacek, K., 2021. Implications of COVID-19 lockdowns on surface passenger mobility and related CO_2 emission changes in Europe. Appl. Energy 300, 117396. https://doi.org/10.1016/J.APENERGY.2021.117396.

Shukla, A.K., Lalchandani, V., Bhattu, D., Dave, J.S., Rai, P., Thamban, N.M., Mishra, S., Gaddamidi, S., Tripathi, N., Vats, P., Rastogi, N., Sahu, L., Ganguly, D., Kumar, M., Singh, V., Gargava, P., Tripathi, S.N., 2021. Real-time quantification and source apportionment of fine particulate matter including organics and elements in Delhi during summertime. Atmos. Environ. 261, 118598. https://doi.org/10.1016/j.atmosenv.2021.118598.

Shukla, A.K., Tripathi, S.N., Canonaco, F., Lalchandani, V., Sahu, R., Srivastava, D., Dave, J., Thamban, N.M., Gaddamidi, S., Sahu, L., Kumar, M., Singh, V., Rastogi, N., 2023. Spatio-temporal variation of C-$PM_{2.5}$ (composition based $PM_{2.5}$) sources using PMF*PMF (double-PMF) and single-combined PMF technique on real-time non-refractory, BC and elemental measurements during post-monsoon and winter at two sites in Delhi, India. Atmos. Environ. 293, 119456. https://doi.org/10.1016/J.ATMOSENV.2022.119456.

Shukla, A.K., Tripathi, S.N., Talukdar, S., Murari, V., Gaddamidi, S., Manousakas, M.I., Lalchandani, V., Dixit, K., Ruge, V.M., Khare, P., Kumar, M., Singh, V., Rastogi, N., Tiwari, S., Srivastava, A.K., Ganguly, D., Daellenbach, K.R., Prévôt, A.S.H., 2025. Measurement report: sources and meteorology influencing highly time-resolved $PM_{2.5}$ trace elements at three urban sites in the extremely polluted indo-gangetic plain in India. Atmos. Chem. Phys. 25, 3765–3784. https://doi.org/10.5194/acp-25-3765-2025.

Silva, E., Huang, S., Lawrence, J., Martins, M.A.G., Li, J., Koutrakis, P., 2021. Trace element concentrations in ambient air as a function of distance from road. J. Air Waste Manag. Assoc. 71, 129–136. https://doi.org/10.1080/10962247.2020.1866711.

Simon, H., Beck, L., Bhave, P.V., Divita, F., Hsu, Y., Luecken, D., David Mobley, J., Pouliot, G.A., Reff, A., Sarwar, G., Strum, M., 2010. The development and uses of EPA's SPECIATE database. Atmos. Pollut. Res. 1, 196–206. https://doi.org/10.5094/APR.2010.026.

Skorbiłowicz, M., Skorbiłowicz, E., Łapiński, W., 2020. Assessment of metallic content, pollution, and sources of road dust in the city of Białystok (Poland). Aerosol Air Qual. Res. 20, 2507–2518. https://doi.org/10.4209/aaqr.2019.10.0518.

Slowik, J.G., Vlasenko, A., McGuire, M., Evans, G.J., Abbatt, J.P.D., 2010. Simultaneous factor analysis of organic particle and gas mass spectra: AMS and PTR-MS measurements at an urban site. Atmos. Chem. Phys. 10, 1969–1988. https://doi.org/10.5194/ACP-10-1969-2010.

Sofowote, U.M., Di Federico, L.M., Healy, R.M., Debosz, J., Su, Y., Wang, J., Munoz, A., 2019. Heavy metals in the near-road environment: results of semi-continuous monitoring of ambient particulate matter in the greater Toronto and Hamilton area. Atmos. Environ. X 1, 100005. https://doi.org/10.1016/j.aeaoa.2019.100005.

Sofowote, U.M., Rastogi, A.K., Debosz, J., Hopke, P.K., 2014. Advanced receptor modeling of near–real–time, ambient $PM_{2.5}$ and its associated components collected at an urban–industrial site in Toronto, Ontario. Atmos. Pollut. Res. 5, 13–23. https://doi.org/10.5094/APR.2014.003.

Sokhi, R.S., Moussiopoulos, N., Baklanov, A., Bartzis, J., Coll, I., Finardi, S., Friedrich, R., Geels, C., Grönholm, T., Halenka, T., Ketzel, M., Maragkidou, A., Matthias, V., Moldanova, J., Ntziachristos, L., Schäfer, K., Suppan, P., Tsegas, G., Carmichael, G., Franco, V., Hanna, S., Jalkanen, J.P., Velders, G.J.M., Kukkonen, J., 2022. Advances in air quality research - current and emerging challenges. Atmos. Chem. Phys. 22, 4615–4703. https://doi.org/10.5194/ACP-22-4615-2022.

Song, S.K., Shon, Z.H., Moon, S.H., Lee, T.H., Kim, H.S., Kang, S.H., Park, G.H., Yoo, E.C., 2022. Impact of international Maritime organization 2020 sulfur content regulations on port air quality at international hub port. J. Clean. Prod. 347, 131298. https://doi.org/10.1016/J.JCLEPRO.2022.131298.

Sorte, S., Rodrigues, V., Borrego, C., Monteiro, A., 2020. Impact of harbour activities on local air quality: a review. Environ. Pollut. 257, 113542. https://doi.org/10.1016/J.ENVPOL.2019.113542.

Sowlat, M.H., Hasheminassab, S., Grant, B., Pakbin, P., Low, J., Polidori, A., 2024. Temporal shifts in sources and composition of particulate metals in an environmental justice community: impacts of continued emission reductions, COVID-19, and wildfires. Atmos. Environ. 336, 120760. https://doi.org/10.1016/J.ATMOSENV.2024.120760.

Spyropoulos, G.C., Nastos, P.T., Moustris, K.P., Chalvatzis, K.J., 2022. Transportation and air quality perspectives and projections in a Mediterranean country, the case of Greece. Land 11, 152. https://doi.org/10.3390/LAND11020152.

Stavroulas, I., Bougiatioti, A., Grivas, G., Liakakou, E., Petrinoli, K., Kourtidis, K., Gerasopoulos, E., Mihalopoulos, N., 2024. Cooking as an organic aerosol source leading to urban air quality degradation. Sci. Total Environ. 908, 168031. https://doi.org/10.1016/J.SCITOTENV.2023.168031.

Stavroulas, I., Bougiatioti, A., Grivas, G., Paraskevopoulou, D., Tsagkaraki, M., Zarmpas, P., Liakakou, E., Gerasopoulos, E., Mihalopoulos, N., 2019. Sources and processes that control the submicron organic aerosol composition in an urban Mediterranean environment (Athens): a high temporal-resolution chemical composition measurement study. Atmos. Chem. Phys. 19, 901–919. https://doi.org/10.5194/acp-19-901-2019.

Stavroulas, I., Grivas, G., Liakakou, E., Kalkavouras, P., Bougiatioti, A., Kaskaoutis, D.G., Lianou, M., Papoutsidaki, K., Tsagkaraki, M., Zarmpas, P., Gerasopoulos, E., Mihalopoulos, N., 2021. Online chemical characterization and sources of submicron aerosol in the major Mediterranean Port City of Piraeus, Greece. Atmosphere 12. https://doi.org/10.3390/ATMOS12121686, 2021 Page 1686 12, 1686.

Stavroulas, I., Grivas, G., Michalopoulos, P., Liakakou, E., Bougiatioti, A., Kalkavouras, P., Fameli, K.M., Hatzianastassiou, N., Mihalopoulos, N., Gerasopoulos, E., 2020. Field evaluation of low-cost PM sensors (Purple Air PA-II) under variable urban air quality conditions, in Greece. Atmosphere 11, 926. https://doi.org/10.3390/ATMOS11090926.

Stavroulas, I., Yus-diez, J., Via, M., Glojek, K., Drinovec, L., Manousakas, I., Prévôt, A., Močnik, G., 2025. Characterization of cooking aerosol through an ensemble of measurements targeting chemical composition, physical properties and oxidative potential. EGU General Assembly. https://doi.org/10.5194/egusphere-egu25-17091, 2025, EGU25-17091.

Stein, A.F., Draxler, R.R., Rolph, G.D., Stunder, B.J.B., Cohen, M.D., Ngan, F., 2015. NOAA's HYSPLIT atmospheric transport and dispersion modeling system. Bull. Am. Meteorol. Soc. 96, 2059–2077. https://doi.org/10.1175/BAMS-D-14-00110.1.

Su, C.P., Peng, X., Huang, X.F., Zeng, L.W., Cao, L.M., Tang, M.X., Chen, Y., Zhu, B., Wang, Y., He, L.Y., 2020. Development and application of a mass closure $PM_{2.5}$ composition online monitoring system. Atmos. Meas. Tech. 13, 5407–5422. https://doi.org/10.5194/AMT-13-5407-2020.

Sun, Y., Luo, H., Li, Y., Zhou, W., Xu, W., Fu, P., Zhao, D., 2025. Atmospheric organic aerosols: online molecular characterization and environmental impacts. npj Clim. Atmos. Sci. 8, 1–16. https://doi.org/10.1038/S41612-025-01199-2.

Theodosi, C., Grivas, G., Zarmpas, P., Chaloulakou, A., Mihalopoulos, N., 2011. Mass and chemical composition of size-segregated aerosols (PM_1, $PM_{2.5}$, PM_1) over Athens, Greece: local versus regional sources. Atmos. Chem. Phys. 11, 11895–11911. https://doi.org/10.5194/acp-11-11895-2011.

Theodosi, C., Tsagkaraki, M., Zarmpas, P., Grivas, G., Liakakou, E., Paraskevopoulou, D., Lianou, M., Gerasopoulos, E., Mihalopoulos, N., 2018. Multi-year chemical composition of the fine-aerosol fraction in Athens, Greece, with emphasis on the contribution of residential heating in wintertime. Atmos. Chem. Phys. 18, 14371–14391. https://doi.org/10.5194/acp-18-14371-2018.

Timmers, V.R.J.H., Achten, P.A.J., 2016. Non-exhaust PM emissions from electric vehicles. Atmos. Environ. 134, 10–17. https://doi.org/10.1016/J.ATMOSENV.2016.03.017.

Tobler, A., Bhattu, D., Canonaco, F., Lalchandani, V., Shukla, A., Thamban, N.M., Mishra, S., Srivastava, A.K., Bisht, D.S., Tiwari, S., Singh, S., Močnik, G., Baltensperger, U., Tripathi, S.N., Slowik, J.G., Prévôt, A.S.H., 2020. Chemical characterization of $PM_{2.5}$ and source apportionment of organic aerosol in New Delhi, India. Sci. Total Environ. 745, 140924. https://doi.org/10.1016/J.SCITOTENV.2020.140924.

Toscano, D., 2023. The impact of shipping on air quality in the port cities of the Mediterranean area: a review. Atmosphere 14, 1180. https://doi.org/10.3390/ATMOS14071180, 2023.

Trebs, I., Lett, C., Krein, A., Matsumoto Kawaguchi, E., Junk, J., 2024. Performance evaluation of an online monitor based on X-ray fluorescence for detecting elemental concentrations in ambient particulate matter. Atmos. Meas. Tech. 17, 6791–6805. https://doi.org/10.5194/AMT-17-6791-2024.

Tremper, A.H., Font, A., Priestman, M., Hamad, S.H., Chung, T.-C., Pribadi, A., Brown, R. J.C., Goddard, S.L., Grassineau, N., Petterson, K., Kelly, F.J., Green, D.C., 2018. Field and laboratory evaluation of a high time resolution X-Ray fluorescence instrument for determining the elemental composition of ambient aerosols. Atmos. Meas. Tech. 11, 3541–3557. https://doi.org/10.5194/amt-11-3541-2018.

Tritsarolis, A., Kontoulis, Y., Theodoridis, Y., 2022. The Piraeus AIS dataset for large-scale maritime data analytics. Data Brief 40, 107782. https://doi.org/10.1016/J.DIB.2021.107782.

Tsai, M.Y., Hoek, G., Eeftens, M., de Hoogh, K., Beelen, R., Beregszászi, T., Cesaroni, G., Cirach, M., Cyrys, J., De Nazelle, A., de Vocht, F., Ducret-Stich, R., Eriksen, K., Galassi, C., Gražuleviciene, R., Gražulevicius, T., Grivas, G., Gryparis, A., Heinrich, J., Hoffmann, B., Iakovides, M., Keuken, M., Krämer, U., Künzli, N., Lanki, T., Madsen, C., Meliefste, K., Merritt, A.S., Mölter, A., Mosler, G., Nieuwenhuijsen, M.J., Pershagen, G., Phuleria, H., Quass, U., Ranzi, A., Schaffner, E., Sokhi, R., Stempfelet, M., Stephanou, E., Sugiri, D., Taimisto, P., Tewis, M., Udvardy, O., Wang, M., Brunekreef, B., 2015. Spatial variation of PM elemental composition between and within 20 European study areas — results of the ESCAPE project. Environ. Int. 84, 181–192. https://doi.org/10.1016/J.ENVINT.2015.04.015.

Tseng, Y.L., Wong, K.W., Yuan, C.S., Lin, C., 2022. Diurnal variation of chemical characteristics and source identification of fine particles in the Kaohsiung Harbor. Aerosol Air Qual. Res. 22, 220100. https://doi.org/10.4209/AAQR.220100.

Tsiodra, I., Grivas, G., Bougiatioti, A., Tavernaraki, K., Parinos, C., Paraskevopoulou, D., Papoutsidaki, K., Tsagkaraki, M., Kozonaki, F.A., Oikonomou, K., Nenes, A., Mihalopoulos, N., 2024. Source apportionment of particle-bound polycyclic aromatic hydrocarbons (PAHs), oxygenated PAHs (OPAHs), and their associated long-term health risks in a major European city. Sci. Total Environ. 951, 175416. https://doi.org/10.1016/J.SCITOTENV.2024.175416.

Tsiodra, I., Grivas, G., Tavernaraki, K., Bougiatioti, A., Apostolaki, M., Paraskevopoulou, D., Gogou, A., Parinos, C., Oikonomou, K., Tsagkaraki, M.,

Zarmpas, P., Nenes, A., Mihalopoulos, N., 2021. Annual exposure to polycyclic aromatic hydrocarbons in urban environments linked to wintertime wood-burning episodes. Atmos. Chem. Phys. 21, 17865–17883. https://doi.org/10.5194/ACP-21-17865-2021.

Tsiodra, I., Grivas, G., Tavernaraki, K., Paraskevopoulou, D., Parinos, C., Tsagkaraki, M., Liakakou, E., Bougiatioti, A., Gerasopoulos, E., Mihalopoulos, N., 2025. Profiling aerosol Polycyclic Aromatic Compounds (PACs) in a severely polluted European city: a comprehensive assessment of the residential biomass burning impact on atmospheric toxicity. J. Hazard Mater. 494, 138431. https://doi.org/10.1016/J.JHAZMAT.2025.138431.

Upadhyay, A., Jiang, J., Cheng, Y., Vasilakos, P., Chen, Y., Banos, D.T., Flückiger, B., Manousakas, M.I., Prévôt, A.S.H., Modini, R.L., de la Campa, A.S., Schemmel, A., Alastuey, A., Bergmans, B., Alves, C.A., Hueglin, C., Colombi, C., Reche, C., Sánchez-Rodas, D., Massabò, D., Diapouli, E., Mazzei, F., Lucarelli, F., Uzu, G., Salma, I., Jaffrezo, J.L., de la Rosa, J.D., Reusser, J.E., Eleftheriadis, K., Alleman, L.Y., Scerri, M., Severi, M., Favez, O., Prati, P., Traversi, R., Vecchi, R., Becagli, S., Nava, S., Castillo, S., Darfeuil, S., Grange, S.K., Querol, X., Kertész, Z., Ciarelli, G., Probst-Hensch, N., Vienneau, D., Kuenen, J., Van Der Gon, H.D., Daellenbach, K.R., Krymova, E., de Hoogh, K., El-Haddad, I., 2025. High-resolution modelling of particulate matter chemical composition over Europe: brake wear pollution. Environ. Int. 202, 109615. https://doi.org/10.1016/J.ENVINT.2025.109615.

Uria-Tellaetxe, I., Carslaw, D.C., 2014. Conditional bivariate probability function for source identification. Environ. Model. Software 59, 1–9. https://doi.org/10.1016/J.ENVSOFT.2014.05.002.

Vasilakopoulou, C.N., Matrali, A., Skyllakou, K., Georgopoulou, M., Aktypis, A., Florou, K., Kaltsonoudis, C., Siouti, E., Kostenidou, E., Błaziak, A., Nenes, A., Papagiannis, S., Eleftheriadis, K., Patoulias, D., Kioutsioukis, I., Pandis, S.N., 2023. Rapid transformation of wildfire emissions to harmful background aerosol. npj Clim. Atmos. Sci. 6, 218. https://doi.org/10.1038/s41612-023-00544-7, 2023.

Vecchi, R., Bernardoni, V., Cricchio, D., D'Alessandro, A., Fermo, P., Lucarelli, F., Nava, S., Piazzalunga, A., Valli, G., 2008. The impact of fireworks on airborne particles. Atmos. Environ. 42, 1121–1132. https://doi.org/10.1016/J.ATMOSENV.2007.10.047.

Veld, M. in t., Alastuey, A., Pandolfi, M., Amato, F., Pérez, N., Reche, C., Via, M., Minguillón, M.C., Escudero, M., Querol, X., 2021. Compositional changes of $PM_{2.5}$ in NE Spain during 2009–2018: a trend analysis of the chemical composition and source apportionment. Sci. Total Environ. 795, 148728. https://doi.org/10.1016/J.SCITOTENV.2021.148728.

Venter, Z.S., Aunan, K., Chowdhury, S., Lelieveld, J., 2020. COVID-19 lockdowns cause global air pollution declines. Proc. Natl. Acad. Sci. 117, 18984–18990. https://doi.org/10.1073/PNAS.2006853117.

Via, M., Yus-Díez, J., Canonaco, F., Petit, J.E., Hopke, P., Reche, C., Pandolfi, M., Ivančič, M., Rigler, M., Prevôt, A.S.H., Querol, X., Alastuey, A., Minguillón, M.C., 2023. Towards a better understanding of fine PM sources: online and offline datasets combination in a single PMF. Environ. Int. 177, 108006. https://doi.org/10.1016/J.ENVINT.2023.108006.

Vieira, J.L., Guimaraes, G.V., De Andre, P.A., Saldiva, P.H.N., Bocchi, E.A., 2016. Effects of reducing exposure to air pollution on submaximal cardiopulmonary test in patients with heart failure: analysis of the randomized, double-blind and controlled FILTER-HF trial. Int. J. Cardiol. 215, 92–97. https://doi.org/10.1016/J.IJCARD.2016.04.071.

Visser, S., Slowik, J.G., Furger, M., Zotter, P., Bukowiecki, N., Dressler, R., Flechsig, U., Appel, K., Green, D.C., Tremper, A.H., Young, D.E., Williams, P.I., Allan, J.D., Herndon, S.C., Williams, L.R., Mohr, C., Xu, L., Ng, N.L., Detournay, A., Barlow, J.F., Halios, C.H., Fleming, Z.L., Baltensperger, U., Prévôt, A.S.H., 2015. Kerb and urban increment of highly time-resolved trace elements in PM_{10}, $PM_{2.5}$ and $PM_{1.0}$ winter aerosol in London during ClearfLo 2012. Atmos. Chem. Phys. 15, 2367–2386. https://doi.org/10.5194/ACP-15-2367-2015.

Vogel, F., Putero, D., Bonasoni, P., Cristofanelli, P., Zanatta, M., Marinoni, A., 2025. Saharan dust transport event characterization in the Mediterranean atmosphere using 21 years of in-situ observations. Atmos. Chem. Phys. 25, 15453–15468. https://doi.org/10.5194/ACP-25-15453-2025.

Wagner, R., Jähn, M., Schepanski, K., 2018. Wildfires as a source of airborne mineral dust - revisiting a conceptual model using large-eddy simulation (LES). Atmos. Chem. Phys. 18, 11863–11884. https://doi.org/10.5194/ACP-18-11863-2018.

Weber, R.J., Orsini, D., Daun, Y., Lee, Y.N., Klotz, P.J., Brechtel, F., 2001. A particle-into-liquid collector for rapid measurement of aerosol bulk chemical composition. Aerosol Sci. Technol. 35, 718–727. https://doi.org/10.1080/02786820152546761.

Wedepohl, K.H., 1995. The composition of the continental crust. Geochem. Cosmochim. Acta 59, 1217–1232. https://doi.org/10.1016/0016-7037(95)00038-2.

Wen, J., Wang, X., Zhang, Y., Zhu, H., Chen, Q., Tian, Y., Shi, X., Shi, G., Feng, Y., 2018. $PM_{2.5}$ source profiles and relative heavy metal risk of ship emissions: source samples from diverse ships, engines, and navigation processes. Atmos. Environ. 191, 55–63. https://doi.org/10.1016/J.ATMOSENV.2018.07.038.

Windell, L.C., Mbengue, S., Pokorná, P., Schwarz, J., Prévôt, A.S.H., Manousakas, M.I., Papagiannis, S., Ondráček, J., Prokeš, R., Ždímal, V., 2025. Xact625i vs. PX-375: a comparative study of online XRF ambient multi-metal monitors vs. ICP-MS. Atmos. Meas. Tech. 18, 7021–7038. https://doi.org/10.5194/AMT-18-7021-2025.

Windell, L.C., Pokorná, P., Schwarz, J., Vodička, P., Hopke, P.K., Zíková, N., Lhotka, R., Ondráček, J., Roztočil, P., Vojtišek, M., Ždímal, V., 2024. Highly time-resolved elemental source apportionment at a Prague urban traffic site. Aerosol Air Qual. Res. 24, 1–17. https://doi.org/10.4209/aaqr.240058.

Wu, S.P., Cai, M.J., Xu, C., Zhang, N., Zhou, J. Bin, Yan, J.P., Schwab, J.J., Yuan, C.S., 2020. Chemical nature of $PM_{2.5}$ and PM_{10} in the coastal urban Xiamen, China: insights into the impacts of shipping emissions and health risk. Atmos. Environ. 227, 117383. https://doi.org/10.1016/J.ATMOSENV.2020.117383.

Wyatt, L.H., Devlin, R.B., Rappold, A.G., Case, M.W., Diaz-Sanchez, D., 2020. Low levels of fine particulate matter increase vascular damage and reduce pulmonary function in young healthy adults. Part. Fibre Toxicol. 17, 1–12. https://doi.org/10.1186/s12989-020-00389-5.

Yu, J., Yan, C., Liu, Y., Li, X., Zhou, T., Zheng, M., 2018. Potassium: a tracer for biomass burning in Beijing? Aerosol Air Qual. Res. 18, 2447–2459. https://doi.org/10.4209/aaqr.2017.11.0536.

Yu, Y., He, S., Wu, X., Zhang, C., Yao, Y., Liao, H., Wang, Q., Xie, M., 2019. $PM_{2.5}$ elements at an urban site in Yangtze River Delta, China: high time-resolved measurement and the application in source apportionment. Environ. Pollut. 253, 1089–1099. https://doi.org/10.1016/j.envpol.2019.07.096.

Zhang, B., Zhou, T., Liu, Y., Yan, C., Li, X., Yu, J., Wang, S., Liu, B., Zheng, M., 2019a. Comparison of water-soluble inorganic ions and trace metals in $PM_{2.5}$ between online and offline measurements in Beijing during winter. Atmos. Pollut. Res. 10, 1755–1765. https://doi.org/10.1016/j.apr.2019.07.007.

Zhang, Y., Favez, O., Petit, J.E., Canonaco, F., Truong, F., Bonnaire, N., Crenn, V., Amodeo, T., Prévôt, A.S.H., Sciare, J., Gros, V., Albinet, A., 2019b. Six-year source apportionment of submicron organic aerosols from near-continuous highly time-resolved measurements at SIRTA (Paris area, France). Atmos. Chem. Phys. 19, 14755–14776. https://doi.org/10.5194/ACP-19-14755-2019.

Zhang, Z., Tao, J., Zhang, L., Hu, B., Liu, M., Nie, F., Lu, H., Chen, L., Wu, Y., Chen, D., Wang, B., Che, H., 2024. Influence of sources and atmospheric processes on metal solubility in $PM_{2.5}$ in urban Guangzhou, South China. Sci. Total Environ. 951, 175807. https://doi.org/10.1016/j.scitotenv.2024.175807.

Zhou, L., Liu, Q., Lee, B.P., Chan, C.K., Hallquist, Å.M., Sjödin, Å., Jerksjö, M., Salberg, H., Wängberg, I., Hallquist, M., Salvador, C.M., Gaita, S.M., Mellqvist, J., 2020. A transition of atmospheric emissions of particles and gases from on-road heavy-duty trucks. Atmos. Chem. Phys. 20, 1701–1722. https://doi.org/10.5194/ACP-20-1701-2020.